# Representation of phosphorus cycle in Joint UK Land Environment Simulator (vn5.5_JULES-CNP)

Mahdi (André) Nakhavali[1], Lina M. Mercado[1,2], Iain P. Hartley[1], Stephen Sitch[1], Fernanda V Cunha[3], Raffaello di Ponzio[3], Laynara F. Lugli[3], Carlos A. Quesada[3], Kelly M. Andersen[1,4,5], Sarah E. Chadburn[6], Andy J. Wiltshire[1,7], Douglas B. Clark[2], Gyovanni Ribeiro[3], Lara Siebert[3], Anna C. M. Moraes[3], Jéssica Schmeisk Rosa[3], Rafael Assis[3] and José L. Camargo[3]

[1]University of Exeter, College of Life and Environmental Sciences, Exeter, EX4 4QE, United Kingdom
[2]UK Centre for Ecology and Hydrology, Wallingford, OX10 8BB, United Kingdom
[3]Coordination of Environmental Dynamics, National Institute of Amazonian Research, Manaus, AM 69060-062, Brazil
[4] University of Edinburgh, School of Geosciences, Edinburgh, EH8 9AB, UK
[5] Nanyang Technological University, Asian School of the Environment, Singapore, 639798, Singapore
[6]College of Engineering, Mathematics, and Physical Sciences, University of Exeter, Exeter, EX4 4QE, United Kingdom
[7]Met Office Hadley Centre, Exeter, Devon, EX1 3PB, United Kingdom

*Correspondence to*: Mahdi (André) Nakhavali (m.nakhavali@exeter.ac.uk)

## Abstract

Most Land Surface Models (LSMs), the land components of Earth system models (ESMs), include representation of nitrogen (N) limitation on ecosystem productivity. However only few of these models have incorporated phosphorus (P) cycling. In tropical ecosystems, this is likely to be important as N tends to be abundant but the availability of rock-derived elements, such as P, can be very low. Thus, without a representation of P cycling, tropical forest response in areas such as Amazonia to rising atmospheric $CO_2$ conditions remains highly uncertain. In this study, we introduced P dynamics and its interactions with the N and carbon (C) cycles into the Joint UK Land Environment Simulator (JULES). The new model (JULES-CNP) includes the representation of P stocks in vegetation and soil pools, as well as key processes controlling fluxes between these pools. We develop and evaluate JULES-CNP using in situ data collected at a low fertility site in the Central Amazon, with a soil P content representative of 60% of soils across the Amazon basin, to parameterise, calibrate and evaluate JULES-CNP. Novel soil and plant P pool observations are used for parameterisation and calibration and the model is evaluated against C fluxes and stocks, and for those soil P pools not used for parameterisation/calibration. We then evaluate the model at additional P limited test sites across the Amazon, in Panama and Hawaii showing a significant improvement over the C and CN only versions of the model. The model is then applied under elevated $CO_2$ (600 ppm) at our study site Central Amazon to quantify the impact of P limitation on $CO_2$ fertilization. We compare our results against current state of the art CNP models using the same methodology that was used in the AmazonFACE model intercomparison study. The model is able to reproduce the observed plant and soil P pools and fluxes used for evaluation under ambient $CO_2$. We estimate P to limit net primary productivity (NPP) by 24% under current $CO_2$ and by 46% under elevated $CO_2$. Under elevated $CO_2$, biomass in simulations accounting for CNP increase by 10% relative to contemporary $CO_2$ conditions, although it is 5% lower compared with CN and C-only simulations. Our results highlight the potential for high P limitation and therefore lower $CO_2$ fertilization capacity in the Amazon forest with low fertility soils.

# 1. Introduction

Land ecosystems currently take up about 30% of anthropogenic $CO_2$ emissions (Friedlingstein *et al.*, 2020), thus buffering the anthropogenic increase in atmospheric $CO_2$. Tropical forests play a major role in the land C cycle, account for about half of global net primary production (NPP)(Schimel *et al.*, 2015), and store the highest above ground carbon among all biomes (Pan *et al.*, 2011; Mitchard, 2018).

The C sink capacity of tropical forests may be constrained by nutrient availability for plant photosynthesis and growth (Vitousek and Howarth, 1991; Elser *et al.*, 2007; LeBauer and Treseder, 2008) via P (Nordin, Högberg and Näsholm, 2001; Shen *et al.*, 2011) and/or N related processes (DeLuca, Keeney and McCarty, 1992; Perakis and Hedin, 2002). Global process-based models of vegetation dynamics and function suggest a continued land C sink in the tropical forests, largely attributed to the $CO_2$ fertilization effect (Sitch *et al.*, 2008; Schimel, Stephens and Fisher, 2015; Koch, Hubau and Lewis, 2021). However, many of these models typically do not consider P constraints on plant growth (Fleischer *et al.*, 2019), which is likely to be an important limiting nutrient in tropical ecosystems, characterised by old and heavily weathered soils. The importance of nutrient cycling representation in Earth System Models (ESMs), and the lack thereof, was highlighted by Hungate *et al.* (2003) and Zaehle and Dalmonech (2011), showing the significance of nitrogen inclusion in ESMs for generating more realistic estimations of the future evolution of the terrestrial C sink. However, in the Coupled Climate C Cycle Model Inter-comparison Project (C4MIP), none of the participating ESMs included N dynamics (Friedlingstein *et al.*, 2006). Seven years later, for the update in CMIP5 (Anav *et al.*, 2013), three models out of eighteen with N dynamics were included (Bentsen *et al.*, 2013; Long *et al.*, 2013; Ji *et al.*, 2014). Although much progress has been made in the inclusion of an N cycle in ESMs so far, none of the CMIP5 models included P cycling and in the most recent CMIP6, only one model includes P (ACCESSESM1.5 model) (Arora *et al.*, 2020).

The long history of soil development in tropical regions which involves the loss of rock-derived nutrients through weathering and leaching on geologic timescales (Vitousek et al., 1997, 2010) results in highly weathered soils. Soil P is hypothesized to be among the key limiting nutrients to plant growth in tropical forests (Vitousek *et al.*, 1997, 2010; Hou *et al.*, 2020), unlike temperate forest where N is hypothesised to be the main constraint (Aerts and Chapin, 1999; Luo *et al.*, 2004). Low P availability in tropical soils is related to the limited un-weathered parent material or organic compounds as source of P (Walker and Syers, 1976), active sorption (Sanchez, 1977) and high occlusion (Yang and Post, 2011) which further reduce plant available P. Although N limitation can impact the terrestrial C sink response to increasing atmospheric $CO_2$ by changing plant C fixation capacity (Luo et al., 2004), this can be partially ameliorated over time by input of N into the biosphere via the continuous inputs of N into ecosystems from atmospheric deposition and biological N fixation (Vitousek et al., 2010). P-limitation is pervasive in natural ecosystems (Hou *et al.*, 2020) and the lack of large P inputs into ecosystems, especially those growing on highly weathered soil, may make P limitation a stronger constraint on ecosystem response to elevated $CO_2$ ($eCO_2$) than N (Gentile et al., 2012; Sardans, Rivas-Ubach and Peñuelas, 2012). This causes considerable uncertainty in predicting the future of the Amazon forest C sink (Yang *et al.*, 2014).

There is evidence to suggest P limitation on plant productivity in the Amazon forest (Malhi, 2012) where it has been shown that the younger, more fertile west and south-west Amazon soils have higher tree turnover (Phillips et al., 2004; Stephenson and Van Mantgem, 2005) and stem growth rates (Malhi *et al.*, 2004) and lower above ground biomass (Baker *et al.*, 2004; Malhi *et al.*, 2006) compared to their central and eastern counterparts. Total soil P has been found as the best predictor of stem growth (Quesada *et al.*, 2010) and of total NPP (Aragão *et al.*, 2009) across this fertility gradient, and foliar P is positively related to plant photosynthetic capacity ($V_{cmax}$ and $J_{cmax}$) in these forests (Mercado *et al.*, 2011).

However, modelling studies are unable to reproduce observed spatial patterns of NPP and biomass in the Amazon , one possible reason being the lack of inclusion of soil P constraints on plant productivity and function (Wang, Law and Pak, 2010; Vicca *et al.*, 2012a; Yang *et al.*, 2014). Nevertheless, some modelling studies have focused on improving process and parameter representation using the observational data of spatial variation in woody biomass residence time (Johnson *et al.*, 2016), soil texture and soil P to parameterise the maximum carboxylation capacity ($V_{cmax}$) (Castanho *et al.*, 2013). Results from these studies successfully represent observed patterns of Amazon forest biomass growth increases with increasing soil fertility. However, the full representation of these interactions and the impact of the soil nutrient availability on biomass productivity is still missing in most of ESMs.

So far, several dynamic global vegetation models have been developed to represent P cycling within the soil (Yang *et al.*, 2013; Haverd *et al.*, 2018) and between plant and soils for tropical forests particularly (Yang *et al.*,

2014; Zhu *et al.*, 2016; Goll *et al.*, 2017). Furthermore, a comprehensive study included several models with C-N-P cycling and their feedbacks on the atmospheric C fixation and biomass growth in Amazon forests under ambient and elevated $CO_2$ conditions ($eCO_2$) (Fleischer *et al.*, 2019). Despite these developments, data to underpin them and their projections, particularly for the tropics, is sparse and remains challenging particularly for the Amazon forest (Reed *et al.*, 2015; Jiang *et al.*, 2019). Moreover, due to the lack of detailed measurements, the P-related processes such as ad/desorption and uptake represented in these models are under-constrained and likely oversimplified, thus the future predictions of Amazon forest responses to $eCO_2$ and climate change are uncertain. To fill this gap, in this study, we use data collected as part of the Amazon Fertilization Experiment (AFEX), the first project that focuses on experimental soil nutrient manipulation in the Amazon, with a comprehensive data collection program covering plant ecophysiology, C stocks and fluxes, soil processes including P stocks. Thus, our model parameterization compared to prior P modelling studies includes detailed P processes representation using the site measurements.

Here, we describe the development and implementation of the terrestrial P cycle in the Joint UK Land Environment Simulator (JULES) (Clark *et al.*, 2011), the land component of the UK Earth System Model (UKESM), following the structure of the prior N cycle development (Wiltshire *et al.*, 2021) and utilising state of the art already tested and implemented descriptions of P cycling in other land surface models (Wang, Houlton and Field, 2007; Zhu *et al.*, 2016; Goll *et al.*, 2017).
The model (JULES-CNP) is parameterized and calibrated using novel in situ P soil and plant data from a well-studied forest site in Central Amazon near to Manaus, Brazil with soil P content representative of 60% of soils across the Amazon basin. The new developed P component estimates the sorption of the soil organic and inorganic P based on the saturation status of the adsorbed P pools, which is unique compared to the other existing P models and enable more realistic estimation of P ad/desorption processes. We first evaluate the model at our study site but also at additional five test sites across the Amazon, in Panama and Hawaii. We then apply the model under ambient and $eCO_2$ following the protocol of Fleischer *et al.*, (2019) to predict nutrient limitations on land biogeochemistry under these conditions. Predictions of the $CO_2$ fertilization effect in JULES-CNP are compared to those in current versions of the model with coupled C and N cycles (JULES-CN) and with C cycle only (JULES-C).

## 2.   Material and methods

### 2.1  JULES

JULES is a process-based model that integrates water, energy, C cycling (JULES-C) (Clark *et al.*, 2011) and N cycling (JULES-CN) (Wiltshire *et al.*, 2021) between the atmosphere, vegetation and soil (Best *et al.*, 2011; Clark *et al.*, 2011). Vegetation dynamics are represented in JULES using the TRIFFID model, using nine distinct plant functional types (PFTs) (tropical and temperate broadleaf evergreen trees, broadleaf deciduous trees, needle-leaf evergreen and deciduous trees, C3 and C4 grasses, and evergreen and deciduous shrubs), as well as height competition (Harper *et al.*, 2016).  Leaf-level photosynthesis (Collatz *et al.*, 1991; Collatz, Ribas-Carbo and Berry, 1992) is scaled to estimate canopy level Gross Primary Productivity (GPP) using a multilayer approach that accounts for vertical variation of radiation interception and partition of sunlit and shaded leaves and associated vertical variation of leaf N and P -exponential decrease through the canopy (Clark *et al.*, 2011:Mercado *et al* 2007, Mercado et al 2009) - while the C:P and N:P ratios remain the same. NPP is estimated as the difference between GPP and autotrophic respiration for each living tissue (leaf, wood, root). NPP is then allocated to increase tissue C stocks and to spread, i.e., expand the fractional coverage of the PFT. The resultant PFT fractional coverages also depend on competition across PFTs for resources, e.g., light. Tissue turnover and vegetation mortality add C into the litter pools. Representation of soil organic C (SOC) follows the Rothamsted Carbon model RothC equations (Jenkinson *et al.*, 1990; Jenkinson and Coleman, 2008) defining four C pools: decomposable plant material (DPM) and resistant plant material (RPM), which receive direct input from litterfall, and microbial biomass (BIO) and humified material (HUM) which receive a fraction of decomposed C from DPM and RPM which is not released to the atmosphere. The limitation of N on SOC is applied to the vegetation and soil components using a dynamic C:N ratio to modify the mineralization and immobilization processes as described in Wiltshire *et al.*, (2021). Note that the soil component of JULES-CN can be run either as a single box model or vertically resolved over soil depth (JULES-CN layered), and in this paper we build upon the vertically resolved version described in Wiltshire et al. (2021).

165
166 ## 2.2 JULES-CNP
167
168 JULES-CNP includes the representation of the P cycle in JULES version (vn5.5) and it is built on existing and
169 well tested representations of P cycling in other global land surface models (Wang, Houlton and Field, 2007;
170 Yang *et al.*, 2014; Goll *et al.*, 2017; Sun *et al.*, 2021). It includes P fluxes within the vegetation and soil
171 components, and the specification of P pools and processes related to P cycling within the soil column (Fig. 1).
172 A parent material pool is introduced to consider the input of weathered P. The adsorbed, desorbed and occluded
173 fractions of P for both organic and inorganic P are also represented. However, except for parent material and
174 occluded P pools, all other pools are estimated at each soil layer. The description of changes in pools and
175 associated relative fluxes are explained in detail in the next sections. Although JULES-CN includes N leaching
176 and deposition, P leaching and deposition are not included in the current version of JULES-CNP.
177
178
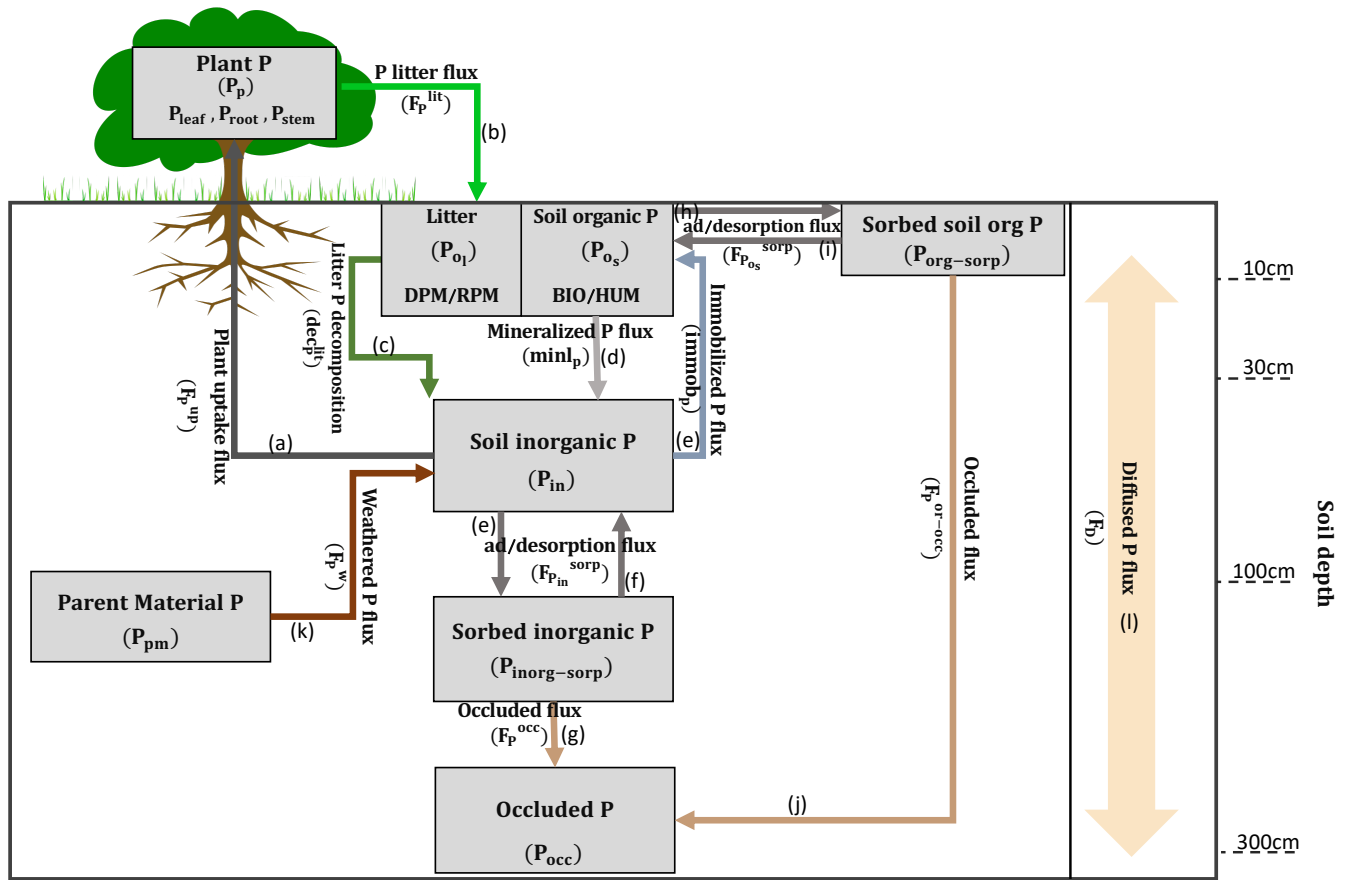
179
180 **Figure.1 – JULES-CNP model scheme including P pools (grey boxes) and fluxes (arrows)**
181
182 ### 2.2.1 P pools
183
184 JULES represents eight P pools comprising organic and inorganic P: plant P ($P_p$) and soil P pools (in each soil
185 layer (n)), litter P ($P_{O_l}$), soil organic P ($P_{O_s}$), soil inorganic P ($P_{in}$), organic sorbed ($P_{org-sorp}$), inorganic sorbed
186 ($P_{inorg-sorp}$), parent material ($P_{pm}$) and occluded ($P_{occ}$) P comprised of both organic and inorganic P. All pools
187 are in units of kg P m$^{-2}$ (Fig 1, Tables 1 and 2).
188
189 Plant P pool is composed of leaf ($P_{leaf}$), fine root ($P_{root}$) and stem together with coarse root ($P_{stem}$), which are
190 related to their associated C pools ($C_{leaf}, C_{root}, C_{stem}$) in (kg C m$^{-2}$) and fixed C to P ratios
191 ($C:P_{leaf}, C:P_{root} C:P_{stem}$) as follows:
192
193 $$P_{leaf} = \frac{C_{leaf}}{C:P_{leaf}}$$ (eq.1)
194

195  $P_{root} = \frac{C_{root}}{C:P_{root}}$  (eq.2)

196

197  $P_{stem} = \frac{C_{stem}}{C:P_{stem}}$  (eq.3)

198

199  Therefore, the plant P pool ($P_p$) is the sum of all vegetation P pools as follows:

200

201  $P_p = P_{leaf} + P_{root} + P_{stem}$  (eq.4)

202

203  Description of the plant P pool ($P_p$) follows Zhu *et al.*, (2016) and is estimated as the difference between the
204  input, plant uptake $F_P^{Up}$ (eq.26) and output of this pool, plant litter flux $F_P^{lit}$ (eq.28), with both fluxes
205  expressed in kg P m$^{-2}$ yr$^{-1}$ as follows:

206

207  $\frac{dP_p}{dt} = F_P^{up} - F_P^{lit}$  (eq.5)

208

209  The litter P pool ($P_{O_l}$) is estimated as a sum of $P_{DPM}$ and $P_{RPM}$ pools over soil layers (n). Each pool is formed by
210  the fluxes of plant litter input ($F_P^{lit}$) and the outgoing decomposed P ($dec_P^{lit}$) both expressed in kg P m$^{-2}$ yr$^{-1}$
211  (eq.28-29). Furthermore, the plant litter input is modified based on the plant type material ratio α (in order to
212  distribute the litter input based on the DPM/RPM fraction) as follows:

213

214  $\frac{dP_{DPM}}{dt} = F_{P_n}^{lit} \times \alpha - dec_{P_{DPM,n}}$  (eq.6)

215

216  $\frac{dP_{RPM}}{dt} = F_{P_n}^{lit} \times (1 - \alpha) - dec_{P_{RPM,n}}$  (eq.7)

217

218  $P_{O_l} = \sum_{n=1}^{N} P_{DPM_n} + \sum_{n=1}^{N} P_{RPM_n}$  (eq.8)

219

220  The soil organic pool ($P_{O_s}$) is represented as the sum of $P_{BIO}$ and $P_{HUM}$. These pools are estimated from the
221  difference between P inputs from total immobilized ($F_{immob_P}$) distributed between BIO and HUM based on
222  fixed fraction (0.46 for BIO, 0.54 for HUM) (Jenkinson *et al.*, 1990; Jenkinson and Coleman, 2008) and
223  desorbed P, $F_{P_{O_S}}^{desorp}$ and P outputs from mineralized ($F_{minl_P}$), and adsorbed P fluxes ($F_{P_{O_S}}^{sorp}$) (adsorption:
224  eq. 40 and desorption: eq.41) with all fluxes expressed in kg P m$^{-2}$ yr$^{-1}$ as follows:

225

226  $\frac{dP_{BIO}}{dt} = 0.46 \times F_{immob_{P_n}} + F_{P_{O_S BIO,n}}^{desorp} - F_{minl_{P BIO,n}} - F_{P_{O_S BIO,n}}^{sorp}$  (eq.9)

227

228  $\frac{dP_{HUM}}{dt} = 0.54 \times F_{immob_{P_n}} + F_{P_{O_S HUM,n}}^{desorp} - F_{minl_{P BIO,n}} - F_{P_{O_S HUM,n}}^{sorp}$  (eq.10)

229

230  $P_{O_s} = \sum_{n=1}^{N} P_{BIO_n} + \sum_{n=1}^{N} P_{HUM_n}$  (eq.11)

231

232

233  Description of the inorganic sorbed P pool ($P_{inorg-sorp}$) follows Wang *et al.*, (2007) and is represented as the
234  difference between the input flux of inorganic sorption ($F_{P_{in}}^{sorp}$) (eq. 37) and output fluxes of inorganic
235  desorption ($F_{P_{in}}^{desorp}$) (eq. 38) and occluded P ($F_P^{occ}$) (eq. 39), with all fluxes expressed in kg P m$^{-2}$ yr$^{-1}$ as
236  follows:

237

238  $\frac{dP_{inorg-sorp}}{dt} = \sum_{n=1}^{N} F_{P_{in_n}}^{sorp} - \sum_{n=1}^{N} F_{P_{in_n}}^{desorp} - \sum_{n=1}^{N} F_{P_n}^{occ}$  (eq.12)

239

240  The description of the occluded ($P_{occ}$) P pool follows Wang *et al.*, (2007) and Hou *et al*., (2019 ) and is
241  represented as the sum of input fluxes of occluded P from both organic ($F_P^{or-occ}$) (eq. 42) and inorganic P
242  pools ($F_P^{occ}$) expressed in kg P m$^{-2}$ yr$^{-1}$, as follows:

243

244  $\frac{dP_{occ}}{dt} = \sum_{n=1}^{N} F_{P_n}^{occ} + \sum_{n=1}^{N} F_{P_n}^{or-occ}$  (eq.13)

245

The description of the organic sorbed P pool ($P_{org-sorp}$) follows Wang *et al.*, (2007) and is represented as the difference between the input flux of organic sorption ($F_{P_{OS_n}}{}^{sorp}$) and output fluxes of organic desorption ($F_{P_{OS_n}}{}^{desorp}$) and occluded P($F_{P_n}{}^{occ}$), with all fluxes expressed in kg P m$^{-2}$ yr$^{-1}$ as follows:

$$\frac{dP_{org-sorp}}{dt} = \sum_{n=1}^{N} F_{P_{OS_n}}{}^{sorp} - \sum_{n=1}^{N} F_{P_{OS_n}}{}^{desorp} - \sum_{n=1}^{N} F_{P_n}{}^{or-occ} \qquad (eq.14)$$

P from parent material ($P_{pm}$) pool follows Wang *et al.*, (2007) and depends on the weathering flux ($F_P{}^w$) (eq. 43) in kg P m$^{-2}$ yr$^{-1}$ as follows:

$$\frac{dP_{pm}}{dt} = -\sum_{n=1}^{N} F_{P_n}{}^w \qquad (eq.15)$$

### 2.2.2. C and P fluxes

NPP in JULES is calculated as the difference between GPP and autotrophic respiration. In JULES-CNP, potential NPP represents the amount of C, available for tissue growth (C density increase) on a unit area, and spreading (vegetation cover increase as a result of reproduction and recruitment), i.e., to increase the area covered by the vegetation type, assuming no nutrient limitation. The reported NPP in the literature often includes other C fluxes related to the exudates, production of volatiles and non-structural carbohydrates (Malhi *et al.*, 2009; Chapin *et al.*, 2011; Walker *et al.*, 2021) which are challenging to measure (Malhi, Doughty and Galbraith, 2011). Therefore, actual NPP is for our purposes equal to Biomass Production (BP), and is calculated as potential NPP minus excess C (lost to the plant through autotrophic respiration), with the latter the C that cannot be used to grow new plant tissue due to insufficient plant nutrient supply. Hence, if the system is limited by the availability of N and/or P, NPP will be adjusted to match the growth that can be supported with the limited N or P supply, with any excess carbohydrate lost through excess C.
The total excess C term ($\psi_t$) (kg C m$^{-2}$ yr$^{-1}$) is calculated as:

$$\psi_t = \psi_g + \psi_s \qquad (eq.16)$$

where $\psi_g$ and $\psi_s$ are the excess C fluxes due to growth (g) and spread (s) and are assumed to be rapidly respired by plants.

Therefore, BP is calculated as the difference between potential NPP ($\Pi_c$) and total excess C:

$$BP = \Pi_c - \psi_t \qquad (eq.17)$$

The litter production in JULES before limitation is estimated as follows:

$$F_{C_n}^{lit} = \gamma_{leaf} C_{leaf} + \gamma_{root} C_{root} + \gamma_{wood} C_{wood} \qquad (eq.18)$$

where $\gamma$ is a temperature dependent turnover rate representing the phenological state (Clark *et al.*, 2011). P limitation is applied on the C litter production similar to the N scheme of JULES (JULES-CN) (Wiltshire *et al.*, 2021). In JULES-CN the N limitation effect on the litter production is captured by estimating the available C for litter production as a difference between the NPP and excess C (Wiltshire *et al.*, 2021).

Similar to other P-enabled models (Yang *et al.*, 2014; Goll *et al.*, 2017), JULES-CNP follows the same structure as its N model component. Description of the plant P and N demand follow Wang *et al.*, (2007) and are represented by the sum of demand ($\emptyset_t$) to sustain growth (P-related: ($\emptyset_{g_P}$), N-related: ($\emptyset_{g_N}$)) and to sustain vegetation spreading (to increment PFT fractional coverage) (P-related: ($\emptyset_{S_P}$), N-related: ($\emptyset_{S_N}$)) and is expressed in (P-related in kg P m$^{-2}$ yr$^{-1}$; N-related in kg N m$^{-2}$ yr$^{-1}$). The total demand for growth ($\emptyset_g$) and spreading ($\emptyset_s$) is controlled by the dominant demand between P ($\emptyset_{g_P}$) and N ($\emptyset_{g_N}$) as follows:

$$\emptyset_t = \emptyset_g + \emptyset_s \qquad (eq.19)$$

301 $$\emptyset_{gP} = \frac{P_p}{C_V}\left(\Pi_c - \frac{dC_v}{dt} - \psi_g\right)$$ (eq.20)

302 $$\emptyset_{sP} = \frac{P_p}{C_V}\left(\Pi_c - \frac{dC_v}{dt} - \psi_s\right)$$ (eq.21)

303 $$\emptyset_{gN} = \frac{N_v}{C_V}\left(\Pi_c - \frac{dC_v}{dt} - \psi_g\right)$$ (eq.22)

304 $$\emptyset_{sN} = \frac{N_v}{C_V}\left(\Pi_c - \frac{dC_v}{dt} - \psi_s\right)$$ (eq.23)

305 $$\emptyset_g = \begin{cases} \emptyset_{gP} & \emptyset_{gP} \times \frac{C_V}{P_p} > \emptyset_{gN} \times \frac{C_V}{N_v} \\ \emptyset_{gN} & \emptyset_{gN} \times \frac{C_V}{N_v} > \emptyset_{gP} \times \frac{C_V}{P_p} \end{cases}$$ (eq.24)

306 $$\emptyset_s = \begin{cases} \emptyset_{sP} & \emptyset_{sP} \times \frac{C_V}{P_p} > \emptyset_{sN} \times \frac{C_V}{N_v} \\ \emptyset_{sN} & \emptyset_{sN} \times \frac{C_V}{N_v} > \emptyset_{sP} \times \frac{C_V}{P_p} \end{cases}$$ (eq.25)

307
308
309 where $\frac{P_p}{C_V}$ is the inverse of whole plant C:P ratio, $\frac{N_v}{C_V}$ is inverse plant C:N ratio, $\frac{dC_v}{dt}$ is rate of change in plant C
310 (see Clark $et\ al.,$ (2011) for more detail), $\Pi_c$ is nutrient-unlimited, or potential, NPP (kg C m$^{-2}$ yr$^{-1}$), $\psi_g$ is excess
311 C due to either P or N limitation for plant growth (kg C m$^{-2}$ yr$^{-1}$) and $\psi_s$ is excess C due to either P or N
312 limitation for vegetation spreading (kg C m$^{-2}$ yr$^{-1}$).

313
314 Equations 20 and 22 are solved by first setting $\psi_g = 0.0$ to find the total plant P (eq. 20) and N demand (eq.22).
315 If the P and N demand for growth are less than the available P and N and fractional coverage ($\lambda$) (NPP fraction
316 used for fractional cover increment; for detail see Wiltshire $et\ al.,$ (2021)) at the considered timestep $\Delta t$ then
317 there is no limitation to growth ($i.e.\ \emptyset_{gP} < \frac{(1-\lambda)P_{avail}}{\Delta t}$; $\emptyset_{gN} < \frac{(1-\lambda)N_{avail}}{\Delta t}$). Where there is limited P and/or N
318 availability, the uptake equals the available P and N ($\emptyset_{gP} = \frac{(1-\lambda)P_{avail}}{\Delta t}$; $\emptyset_{gN} = \frac{(1-\lambda)N_{avail}}{\Delta t}$), and the plant
319 growth which cannot be achieved due to nutrient constraints will be deducted from potential NPP, here termed
320 excess C term ($\psi_g$), to give an actual NPP. Following Wiltshire et al., 2021, we assume excess C is respired by
321 the plant.

322
323 Similarly, in order to estimate the P and N demand for spreading (eq. 21 and 23), initially the excess C from
324 spreading is set to 0.0 ($\psi_s = 0.0$), i.e under the assumption that there is no nutrient limitation. If the P and N
325 demand for spreading are lower than the available P and N and fractional coverage ($\lambda$) ($\emptyset_{SP} <$
326 $\frac{(1-\lambda)P_{avail}}{\Delta t}$; $\emptyset_{SN} < \frac{(1-\lambda)N_{avail}}{\Delta t}$), then there is no limitation on spreading and in case of limited P and N
327 availability, the uptake equals the available P and N ($\emptyset_{SP} = \frac{(1-\lambda)P_{avail}}{\Delta t}$; $\emptyset_{SN} = \frac{(1-\lambda)N_{avail}}{\Delta t}$), and the excess C
328 for spread ($\psi_s$) is subtracted from potential NPP.

329
330 Plant P uptake ($F_p{}^{up}$) (arrow a in Fig 1) is estimated based on the P demand for growth and spreading ($\emptyset_t$) and
331 the root uptake capacity ($u^{max}$) (kg P kg$^{-1}$ C yr$^{-1}$), as follows:

332
333 $$F_p{}^{up}{}_n = \begin{cases} \emptyset_t & \emptyset_t \leq u^{max} \\ u^{max} & \emptyset_t > u^{max} \end{cases}$$ (eq.26)

334
335 Plant P uptake ($F_p{}^{up}$) varies spatially depending on the root uptake capacity ($u^{max}$) followed by Goll $et\ al.,$
336 (2017). Therefore, in regions with limited P supply, the plant P uptake is limited to the $u^{max}$ and consequently
337 impacts the excess C and BP.
338 The root uptake capacity depends on the maximum root uptake capacity ($v_{max}$) (kg P kg$^{-1}$ C yr$^{-1}$), root depth
339 ($d_{root}$), the concentration of inorganic P at different soil depths ($P_{in}$), and a half saturation term at which half of
340 the maximum uptake capacity is reached using inorganic P at different soil depths ($P_{in}$), a scaling uptake ratio
341 ($K_p$) ($\mu$mol P l$^{-1}$), unit conversion ($C_f$) (1 kg P$^{-1}$), and soil moisture ($\theta$) (l m$^{-2}$), as follows:

342
343 $$u^{max} = v_{max} \times d_{root} \times \sum_{n=1}^{N} P_{in_n} \times \left(\frac{1}{\sum_{n=1}^{N} P_{in_n} + c_f \times K_p \times \theta_n}\right)$$ (eq.27)

344

Description of the litter production of P ($F_{P_n}^{lit}$) (arrow b in Fig 1) follows JULES-CN as in Wiltshire $et\ al.$, (2021) and is calculated based on the litter flux of C (kg C m$^{-2}$ yr$^{-1}$) using leaf, root and wood turnovers (yr$^{-1}$), and through the vegetation dynamics due to large-scale disturbance and litter production density, as follows:

$$F_{P_n}^{lit} = \left(\frac{(1-k_{leaf})\gamma_{leaf}C_{leaf}}{C:P_{leaf}}\right) + \left(\frac{(1-k_{root})\gamma_{root}C_{root}}{C:P_{root}}\right) + \left(\frac{\gamma_{wood}C_{wood}}{C:P_{stem}}\right) \quad \text{(eq.28)}$$

where $\lambda$ is the leaf, root and stem re-translocation (at daily timestep) coefficient (Zaehle and Friend, 2010; Clark $et\ al.$, 2011) and the related $C:P$ ratios for P fraction and $\gamma$ is a temperature dependent turnover rate representing the phenological state (Clark $et\ al.$, 2011).

The decomposition of litter ($dec^{lit}$) (arrow c in Fig 1) depends on soil respiration ($R$) (kg C m$^{-2}$ yr$^{-1}$), the litter C:P ratio ($C:P_{lit}$) at each soil layer (n) as follows:

$$dec_P^{lit} = \frac{\sum_{n=1}^{N} R_n}{C:P_{lit}} \quad \text{(eq.29)}$$

where the $C:P_{lit}$ is calculated based on litter C pool (DPM and RPM) ($lit^C$) (kg C m$^{-2}$ yr$^{-1}$) and litter P pool ($P_{O_l}$) as follows:

$$C:P_{lit} = \frac{\sum_{n=1}^{N} lit_n^C}{P_{O_{l_n}}} \quad \text{(eq.30)}$$

The mineralized ($F_{minl_P}$) (arrow d in Fig 1) and immobilized ($F_{immob_P}$) (arrow e in Fig 1) P fluxes are calculated based on C mineralization and immobilization, C:P ratios of plant (i) (DPM/RPM) ($C:P_{plant}$) and soil (HUM/BIO) ($C:P_{soil}$), soil pool potential respiration ($R_{POT_i}$) (kg C m$^{-2}$ yr$^{-1}$) and the respiration partitioning fraction ($resp\_frac$) as follows:

$$F_{minl_{P_n}} = \frac{\sum_{n=1}^{N} R_{POT_{i,n}}}{C:P_{plant}} \quad \text{(eq.31)}$$

$$F_{immob_{P_n}} = \frac{\sum_{n=1}^{N} R_{i,n} \times resp\_frac}{C:P_{soil}} \quad \text{(eq.32)}$$

The soil respiration from each soil layer ($R_{i,n}$) is estimated from potential soil respiration ($R_{POT_{i,n}}$) for the DPM, RPM pools and the litter decomposition rate modifier ($F_{P_n}$) as follows:

$$R_{i,n} = R_{POT_{i,n}} \times F_{P_n} \quad \text{(eq.33)}$$

where the description of $F_{P_n}$ for P pools ($F_{P_{P_n}}$) follows Wang $et\ al.$,(2007) and is estimated based on the soil pool (BIO/HUM) mineralization ($minl_{P-BIO_n}$, $minl_{P-HUM_n}$) and immobilization ($immob_{P-BIO_n}$, $immob_{P-HUM_n}$) (in kg P m$^{-2}$ yr$^{-1}$), soil inorganic P ($P_{inorg_n}$) (in kg P m$^{-2}$), and litter pools (DPM/RPM) demand (in kg P m$^{-2}$ yr$^{-1}$) as follows:

$$F_{P_{P_n}} = \frac{(minl_{P-BIO_n}+minl_{P-HUM_n}-immob_{P-BIO_n}-immob_{P-HUM_n})+P_{inorg_n}}{DEM_{DPM_n}+DEM_{RPM_n}} \quad \text{(eq.34)}$$

The net demand associated with decomposition of litter pools ($DEM_{k,n}$) represents the P required by microbes which convert DPM and RPM into BIO and HUM. The limitation due to insufficient P availability is estimated based on the potential mineralization ($minl_{p-pot}$) and immobilization ($immob_{p-pot}$) (in kg P m$^{-2}$ yr$^{-1}$) of pools (k) as follows:

$$DEM_{k,n} = immob_{p-pot,k} - minl_{p-pot,k} \quad \text{(eq.35)}$$

The $F_{P_n}$ estimated for N pools ($F_{P_{N_n}}$) follows the same formulation as P (see Wiltshire $et\ al.$, 2021 for further details) and the $F_{P_n}$ is estimated based on a higher rate modifier between N and P as follows:

397 $$F_{P_n} = \begin{cases} F_{P_{P_n}} & F_{P_{P_n}} > F_{P_{N_n}} \\ F_{P_{N_n}} & F_{P_{N_n}} > F_{P_{P_n}} \end{cases}$$ (eq.36)

398

399 Description of the fluxes of adsorption ($F_{P_{in_n}}{}^{sorp}$) (arrow e in Fig 1) and desorption ($F_{P_{in_n}}{}^{desorp}$) (arrow f in Fig

400 1) of inorganic P in kg P m$^{-2}$ yr$^1$ follow Wang *et al.*, (2010) and are calculated based on soil inorganic ($P_{in_n}$) and

401 sorbed inorganic ($P_{inorg-sorbed_n}$) P pools and inorganic adsorption ($K_{sorp-in}$), desorption ($K_{desorp-in}$)

402 coefficients (kg P m$^{-2}$ yr$^{-1}$) and maximum sorbed inorganic ($P_{in-max}$) (kg P m$^{-2}$) as follows:

403

404 $$F_{P_{in_n}}{}^{sorp} = P_{in_n} \times K_{sorp-in} \times \frac{\left(P_{in-max_n} - P_{inorg-sorbed_n}\right)}{P_{in-max_n}}$$ (eq.37)

405

406 $$F_{P_{in_n}}{}^{desorp} = P_{inorg-sorbed_n} \times K_{desorp-in}$$ (eq.38)

407

408 Description of the occluded inorganic P flux ($F_{P_n}{}^{occ}$) (arrow g in Fig 1) follows Wang *et al.*, (2007) and Hou *et*

409 *al.*, (2019) and is calculated based on sorbed inorganic P pool and P occlusion rate ($K_{occ}$) (kg P m$^{-2}$ yr$^{-1}$) as

410 follows:

411

412 $$F_{P_n}{}^{occ} = P_{inorg-sorbed_n} \times K_{occ}$$ (eq.39)

413

414 Description of the fluxes of adsorption ($F_{P_{O_{S_n}}}{}^{sorp}$) (arrow h in Fig 1) and desorption ($F_{P_{O_{S_n}}}{}^{desorp}$) (arrow i in Fig

415 1) of organic P follow Wang *et al.*, (2010) are calculated based on soil organic and sorbed organic P pools and

416 organic adsorption ($K_{sorp-or}$) (kg P m$^{-2}$ yr$^{-1}$), desorption ($K_{desorp-or}$) coefficients (kg P m$^{-2}$ yr$^{-1}$) and maximum

417 sorbed organic ($P_{org-max}$) (which corresponds to the sorbed soil P saturation, thus modifying the sorption rate

418 respectively) (kg P m$^{-2}$) as follows:

419

420 $$F_{P_{O_{S_n}}}{}^{sorp} = P_{O_{S_n}} \times K_{sorp-or} \times \frac{\left(P_{or-max_n} - P_{org-sorbed_n}\right)}{P_{or-max_n}}$$ (eq.40)

421

422 $$F_{P_{O_{S_n}}}{}^{desorp} = P_{org-sorbed_n} \times K_{desorp-or}$$ (eq.41)

423

424 Description of the occluded organic P flux ($F_{P_n}{}^{or-occ}$) (kg P m$^{-2}$ yr$^{-1}$) (arrow j in Fig 1) follows Wang *et al.*,

425 (2007) and Hou *et al.*, (2019) is calculated based on sorbed organic P pool ($P_{org-sorbed_n}$) and P occlude rate

426 ($K_{occ}$) (kg P m$^{-2}$ yr$^{-1}$) as follows:

427

428 $$F_{P_n}{}^{or-occ} = P_{org-sorbed_n} \times K_{occ}$$ (eq.42)

429

430 Description of the P flux from weathered parent material ($F_{P_n}{}^{w}$) (arrow k in Fig 1) follows Wang *et al.*, (2007)

431 and is calculated based on amount of P in the parent material ($P_{pm}$) and P weathering rate ($K_w$) (kg P m$^{-2}$ yr$^{-1}$) as

432 follows:

433

434 $$F_{P_n}{}^{w} = P_{pm_n} \times K_w$$ (eq.43)

435

436 Description of P diffusion between soil layers ($F_{D_n}$) expressed in (kg P m$^{-2}$ yr$^{-1}$) (arrow l in Fig 1) follows Goll

437 *et al.*, (2017) and is calculated following Fick's second law and it is a function of the diffusion coefficient ($Dz$)

438 in m$^2$ s$^{-1}$, the concentration of inorganic P at different soil depths ($P_{in}$) in kg P m$^{-2}$, the distance ($z$) between the

439 midpoints of soil layers in metres and seconds to year unit conversion ($Yr$):

440

441 $$F_{D_n} = \frac{\partial}{\partial z}\left(D_{z_n} \frac{\partial P_{s_n}}{\partial z}\right) \times Yr$$ (eq.44)

442

443

444

445

446

**Table 1.** Model variables

| Variable | Unit | Definition |
| --- | --- | --- |
| $\psi$ | kg C m$^{-2}$ yr$^{-1}$ | Excess C flux |
| $\emptyset$ | kg P m$^{-2}$ yr$^{-1}$ | Plant demand for uptake |
| $\Pi_c$ | kg C m$^{-2}$ yr$^{-1}$ | Potential NPP |
| $u^{max}$ | kg P kg$^{-1}$ C yr$^{-1}$ | Root uptake capacity |
| $DEM$ | kg P m$^{-2}$ yr$^{-1}$ | Plant pool P associated decomposition demand |
| $dec_P{}^{lit}$ | kg P m$^{-2}$ yr$^{-1}$ | Litter decomposition |
| $F_D$ | kg P m$^{-2}$ yr$^{-1}$ | Plant diffusion flux |
| $F_P$ | - | Plant litter decomposition rate modifier |
| $F_p{}^{lit}$ | kg P m$^{-2}$ yr$^{-1}$ | Plant litter flux |
| $F_p{}^{up}$ | kg P m$^{-2}$ yr$^{-1}$ | Plant uptake |
| $F_{P_{O_S}}{}^{sorp}$ | kg P m$^{-2}$ yr$^{-1}$ | Sorbed organic P flux |
| $F_{P_{in}}{}^{sorp}$ | kg P m$^{-2}$ yr$^{-1}$ | Sorbed inorganic P flux |
| $F_{P_{O_S}}{}^{desorp}$ | kg P m$^{-2}$ yr$^{-1}$ | Desorbed organic P flux |
| $F_{P_{in}}{}^{desorp}$ | kg P m$^{-2}$ yr$^{-1}$ | Desorbed inorganic P flux |
| $F_p{}^{occ}$ | kg P m$^{-2}$ yr$^{-1}$ | Occluded inorganic P flux |
| $F_p{}^{or\text{-}occ}$ | kg P m$^{-2}$ yr$^{-1}$ | Occluded organic P flux |
| $F_p{}^w$ | kg P m$^{-2}$ yr$^{-1}$ | Weathered P flux |
| $F_{immob_P}$ | kg P m$^{-2}$ yr$^{-1}$ | Immobilized P flux |
| $lit_C$ | kg C m$^{-2}$ yr$^{-1}$ | C litter flux |
| $lit_{frac}$ | - | Litter fraction |
| $lit_{leaf}$ | kg C m$^{-2}$ yr$^{-1}$ | Leaf litter flux |
| $lit_{root}$ | kg C m$^{-2}$ yr$^{-1}$ | Root litter flux |
| $lit_{wood}$ | kg C m$^{-2}$ yr$^{-1}$ | Woody litter flux |
| $F_{minl_P}$ | kg P m$^{-2}$ yr$^{-1}$ | Mineralized P flux |
| $P_p$ | kg P m$^{-2}$ | Plant P pool |
| $P_{O_l}$ | kg P m$^{-2}$ | Litter organic pool |
| $P_{O_s}$ | kg P m$^{-2}$ | Soil organic pool |
| $P_{in}$ | kg P m$^{-2}$ | Soil inorganic pool |
| $P_{inorg-sorp}$ | kg P m$^{-2}$ | Soil inorganic sorbed pool |
| $P_{org-sorp}$ | kg P m$^{-2}$ | Soil organic sorbed pool |
| $P_{occ}$ | kg P m$^{-2}$ | Soil occluded pool |
| $P_{pm}$ | kg P m$^{-2}$ | Parent material pool |
| $R$ | kg C m$^{-2}$ yr$^{-1}$ | Total respiration |
| $R_{POT}$ | kg C m$^{-2}$ yr$^{-1}$ | Total potential respiration |
| $R^s$ | kg C m$^{-2}$ yr$^{-1}$ | Soil respiration |
| $R_d$ | kg C m$^{-2}$ yr$^{-1}$ | Leaf dark respiration |
| $T_{ref}$ | K | Soil reference temperature |
| $T_s$ | K | Soil temperature |
| Veg$_c$ | kg C m$^{-2}$ | Sum of biomass |
| z | m | Soil depth |

454
455 **Table 2.** P Model parameters

| Parameter | Value | Unit | Eq. | Description | Source |
|---|---|---|---|---|---|
| **C and N related** | | | | | |
| $\alpha$ | 0.25 | - | 6 | Plant type material ratio | (Clark *et al.*, 2011) |
| $a_{wl}$ | 1.204 | kg C m$^{-2}$ | 50 | Allometric coefficient | calibrated |
| $\sigma_l$ | 0.0375 | kg C m$^{-2}$ per unit LAI | 48 | Specific leaf density | Clark *et al.*, 2011 |
| $b_{wl}$ | 1.667 | - | 50 | Allometric exponent. | Clark *et al.*, 2011 |
| $f_{dr}$ | 0.005 | - | 47 | Respiration scale factor | Calibrated |
| $resp\_frac$ | 0.25 | - | 32 | Respiration fraction | (Clark *et al.*, 2011) |
| $k_{leaf}$ | 0.5 | - | 28 | Leaf N re-translocation coefficient | (Zaehle and Friend, 2010) |
| $k_{root}$ | 0.2 | - | 28 | Root N re-translocation coefficient | (Zaehle and Friend, 2010) |
| $d_{root}$ | 3.0 | - | 27 | Root fraction in each soil layer | (Clark *et al.*, 2011) |
| $v_{int}$ | 7.21 | μmol CO$_2$ m$^{-2}$ s$^{-1}$ | 45 | Intercept in the linear regression between $V_{cmax}$ and $N_{area}$ | Calibrated (Clark *et al.*, 2011) |
| $v_{sl}$ | 19.22 | μmol CO$_2$ gN$^{-1}$ s-1 | 45 | Slope in the linear regression between $V_{cmax}$ and $N_{area}$ | Calibrated (Clark *et al.*, 2011) |
| $LMA$ | 131.571852 | g m-2 | 45 | Observed Leaf Mass per Area | Study site |
| $Leaf\ N$ | 1.79007596 | g g-1 | 45, 46 | Foliar N concentrations | Study site |
| **P related** | | | | | |
| $C{:}P_{soil}$ | 1299.6 | - | 32 | Soil C:P ratio | (Fleischer *et al.*, 2019) |
| $v_{max}$ | 0.0007 | kg P kg$^{-1}$ C yr$^{-1}$ | 27 | Maximum root uptake capacity | Calibrated (Goll *et al.*, 2017) |
| $P$ | 0.7083062 | g kg$^{-1}$ | 46 | Foliar P concentrations | Study site |
| $c_f$ | 3.1×10$^{-5}$ | 1 kg P$^{-1}$ | 27 | Conversion factor | (Goll *et al.*, 2017) |
| $D_z$ | 0.001 | m$^2$ s$^{-1}$ | 44 | Diffusion coefficient | (Burke *et al*, 2017) |
| $K_{occ}$ | 1.2×10$^{-5}$ | yr$^{-1}$ | 39, 42 | P occlusion rate | (Yang *et al.*, 2014) |
| $K_p$ | 3.0 | kg P l$^{-1}$ | 27 | Scaling uptake ratio | Calibrated |
| $K_{sorp-in}$ | 0.0054 | kg P m$^{-2}$ yr$^{-1}$ | 37 | Inorganic P adsorption coefficient | Calibrated (Hou *et al.*, 2019) |
| $K_{sorp-or}$ | 0.00054 | kg P m$^{-2}$ yr$^{-1}$ | 40 | Organic P adsorption coefficient | Calibrated |
| $K_{in-max}$ | 0.0075 | kg P m$^{-2}$ yr$^{-1}$ | 37 | Maximum sorbed inorganic P | Study site |
| $K_{or-max}$ | 0.0042 | kg P m$^{-2}$ yr$^{-1}$ | 40 | Maximum sorbed organic P | Study site |
| $K_w$ | 3×10$^{-6}$ | kg P m$^{-2}$ yr$^{-1}$ | 43 | P weathering rate | (Wang *et al.*, 2010) |

456
457 **2.3 Study sites**
458
459 This study primarily uses data from two nearby sites in Central Amazon in Manaus, Brazil. The main site from
460 here on termed *study site* (2°35′′21.08′′ S, 60°06′′53.63′′ W) (Lugli *et al.*, 2020) is for model development and
461 evaluation. The second site is the Manaus K34 flux site (2°36′′32.67′′ S, 60°12′′33.48′′ W) which provides
462 meteorological station data for running the model but also provides data for model evaluation. Our *study site* is
463 the main lowland tropical forest site maintained by the National Institute for Amazon Research (INPA).
464 Research at this site focuses on projects, combining experimental approaches (Keller *et al.*, 2004; Malhi *et al.*,
465 2009) with modelling (Lapola and Norby, 2014). We use detailed novel soil and plant P pool data from the *study*
466 *site* (Lugli *et al.*, 2020, 2021) for model parameterisation and calibration and carbon stock data for model
467 validation. The *study site* has a very similar forest, geomorphology, soil chemistry and species composition to
468 the well-known and studied K34 flux site (Araújo *et al.*, 2002). The average reported annual precipitation is
469 2431 (mm yr$^{-1}$), with a monthly range of 95 to 304 (mm month$^{-1}$), and averaged temperature is 26°C (Araújo *et*
470 *al.*, 2002). Soil type at this site is Geric Ferrosol with a high clay content and weathering activities (Malhi *et al.*,
471 2004).
472

473 In addition to the *study site* we use data from other P limited locations from the Amazon, Panama and Hawaii
474 (Table 3) for model evaluation. Old-growth forest sites in the Amazon are located across a fertility gradient
475 from west to east (AGP-01, SA3, CAX,) with detailed C cycle measurements available (Aragão *et al.*, (2009)).
476 The site in Panama is located in the Gigante Peninsula in the Barro Colorado Nature Reserve and is a 200 year
477 old semi-deciduous rainforest (Wright *et al.*, 2011) growing on Oxisols developed on Miocene basalt (Dieter,
478 Elsenbeer and Turner, 2010) with the topsoil a dominant clay texture (Turner and Condron, 2013). It is the
479 location of a long term running nutrient fertilization experiment since 1998 (Mirabello *et al.*, 2013). The site in
480 Hawaii (Hawaii Kokee) is a P limited chronosequence that developed on the 4 million year old oxisols soil
481 (Vitousek, 2004) and has a long term fertilization experiment. Site information is provided in Table 3.
482
483 **Table 3.** Test sites name, location and climate characterises.

| Site | Name | Location | | Climate | |
|---|---|---|---|---|---|
| | | Lat. | Lon. | Rainfall (mm yr$^{-1}$) | Temperature(°C) |
| *Study site* | AFEX project | -2.58 | -60.11 | 2431 | 26 |
| **AGP-01** | Agua pudre plot E | -3.72 | -70.3 | 2723 | 25.5 |
| **CAX** | Caxiuanã flux tower site | -1.72 | -51.5 | 2314 | 26.9 |
| **SA3** | Tapajós flux tower site | -2.5 | -55 | 1968 | 26.1 |
| **Gig. Pen.** | Gigante peninsula (control data) | -9.1 | -79.84 | 2600 | 26 |
| **Hawaii K.** | Hawaii Kokee (control data) | 22.13 | -159.62 | 2500 | 16 |

484
485
486 **2.4 Model parameterisation, calibration and evaluation at study site**
487
488 We use observations from the four control plots of the study site to parameterise, calibrate and evaluate different
489 processes in JULES (Table 4). The observations were collected at 4 soil depths and processed using the Hedley
490 sequential fractionation (Hedley, Stewart and Chauhan, 1982; Quesada *et al.*, 2010). Observed Leaf Mass per
491 Area (LMA), leaf N and leaf P estimated from fresh leaves were used as input parameters to JULES to estimate
492 photosynthetic capacity and respiration parameters. JULES vn5.5 (JULES CN in this study) estimates $V_{cmax}$
493 (µmol m$^{-2}$ s$^{-2}$) based on Kattge et al. (2009) using foliar N concentrations in area basis ($nleaf$), as follows:
494
495 $$V_{cmax} = v_{int} + v_{sl} * nleaf \qquad \text{(eq.45)}$$
496
497 where $v_{int}$ is the estimated intercept and $v_{sl}$ is the slope of the linear regression derived for the $V_{cmax}$ estimation.
498 We incorporated an additional P dependency on the estimation of $V_{cmax}$ following Walker et al. (2014) as
499 follows:
500
501 $$\ln(V_{cmax}) = 3.946 + 0.921 \ln(N) + 0.121 \ln(P) + 0.282 \ln(N) \ln(P) \qquad \text{(eq.46)}$$
502
503 Where N and P are foliar concentrations in area basis.
504
505 Implementation of eq. 46 resulted in higher $V_{cmax}$ than in the original version of JULES. A higher $V_{cmax}$ predicted
506 higher leaf and plant respiration (eq.47). Constrained by observations of NPP and plant respiration at the study
507 site, we modified one of the most uncertain parameters in the description of plant respiration ($f_{dr}$) (eq.47) which
508 is the scale factor for leaf dark respiration ($R_d$) as follows:
509
510 $$R_d = f_{dr} V_{cmax} \qquad \text{(eq.47)}$$
511
512 The default value is 0.01 (Clark *et al.*, 2011), and for JULES-CNP simulations at our study site it was modified
513 to 0.005.
514 Observations of aboveground biomass were used to calibrate the non PFT dependent allometric relationships in
515 JULES (Clark et al 2011) (eq 48-50) for leaf, root and wood C. Specifically, the $a_{wl}$ parameter (eq 50) was
516 modified from 0.65 to 1.204 to match better tropical forest allometry:
517
518 $$C_{leaf} = \sigma_l L_b \qquad \text{(eq.48)}$$
519 $$C_{root} = C_{leaf} \qquad \text{(eq.49)}$$

520   $C_{stem} = a_{wl} L_b{}^{b_{wl}}$                                                                                    (eq.50)
521
522   Where $\sigma_l$ is specific leaf density (kg C m$^{-2}$ per unit LAI), $L_b$ is balanced (or seasonal maximum) leaf area index
523   (m$^2$ m$^{-2}$), $a_{wl}$ is allometric coefficient (kg C m$^{-2}$) and $b_{wl}$ is the allometric exponent.
524   Note that JULES-CNP uses the C3 and C4 photosynthesis model from Collatz et al., 1991; Collatz, Ribas-Carbo
525   and Berry, 1992, which does not include estimation of J$_{max}$.
526
527   JULES-CNP has fixed stoichiometry and C:P ratios of leaf and root (measured), and wood (estimated from fresh
528   coarse wood (Lugli, 2013)) which were taken from the *study site* and prescribed in JULES to simulate P
529   dynamics in the plant. The following belowground data were used to represent various soil P pools: Resin and
530   bicarbonate inorganic P (inorganic P: $P_{in}$), organic bicarbonate P (organic P: $P_{O_S}$), NaOH organic P (sorbed
531   organic P: $P_{org-sorp}$), NaOH inorganic P (sorbed inorganic P: $P_{inorg-sorp}$), residual P (occluded P: $P_{occ}$) and
532   HCL P (parent material P: $P_{pm}$) (Table 4). The measurements were collected between 2017 and 2018 in control
533   plots. All measurements were conducted in four soil layers (0-5 ,5-10, 10-20, 20-30 cm). However, to be
534   consistent with the JULES model soil layer discretization scheme, we defined 4 soil layers (0-10 cm, 10-30 cm,
535   30-100 cm and 100-300 cm) and we used the average between 0 and 30 cm to compare against the measurement
536   from the same depth for model evaluation.
537   Vegetation C stocks were derived based on tree diameter measurements at breast height, that are linked to
538   allometric equations and wood density databases to estimate the C stored in each individual tree, and then scaled
539   to the plot (Chave *et al.*, 2014).
540
541   The organic and inorganic soil P was assumed to be always at equilibrium with the relative sorbed pools (Wang,
542   Law and Pak, 2010). Thus, in order to cap P sorption and uptake capacity, the maximum sorption capacities
543   ($P_{in-max_n}$, $P_{or-max_n}$, eq.37 and 39) (adopted from (Wang, Houlton and Field, 2007)) were prescribed using
544   maximum observed sorbed inorganic and organic P. Hence, the maximum sorption capacity defines the
545   equilibrium state of sorbed and free-soil P. Moreover, despite the initial representation of the parent material
546   pool in JULES and its depletion through weathering (eq. 43), as the magnitude of changes in the occluded and
547   parent material pools are insignificant over a short-term (20 years) simulation period (Vitousek *et al.*, 1997),
548   these two pools were prescribed using observations. Remaining parameters used to describe soil P fluxes (eqn.s
549   27-44) were prescribed using values from the literature (Table 4).
550
551   We used a combination of data from the *study site* and the nearby K34 site for model evaluation of C fluxes
552   (GPP, NPP) and C pools (soil and vegetation C, leaf, root and wood C) with no calibration of plant and soil
553   organic and soil inorganic P pools included (Table 4).
554
555   **Table 4.** Observations from study site (taken during 2017-2018) and from Manaus site K34 used for model parameterisation
556   and evaluation

| Process | Variables | Purpose of use | Reference and site |
|---|---|---|---|
| C associated | GPP | Evaluation | Fleischer et al., 2019, K34 |
| | NPP | Evaluation | Fleischer et al., 2019, K34 |
| | Soil C | Evaluation | Malhi et al., 2009, K34 |
| | CUE | Evaluation | Malhi et al., 2009, K34 |
| | Veg C | Evaluation | Study site |
| | Leaf C | Evaluation | Study site |
| | Wood C | Evaluation | Study site |
| | Root C | Evaluation | Study site |
| | LAI | Initialisation | Study site |
| | LMA | Parameterisation | Study site |
| P associated | Resin | Evaluation | Study site |
| | Pi Bic | Evaluation | Study site |
| | Po Bic | Evaluation | Study site |
| | Po NaOH | Calibration | Study site |
| | Pi NaOH | Calibration | Study site |
| | P residual | Parameterisation | Study site |
| | P HCL | Parameterisation | Study site |
| | Leaf N | Parameterisation | Study site |
| | Leaf P | Parameterisation | Study site |
| | Root P | Parameterisation | Study site |
| | Plant C:P ratio | Parameterisation | Study site |

557 **2.4.1    Model parameterisation and evaluation at test sites**
558
559 JULES-CNP was parameterised using reported C:P ratios and maximum sorbed organic and inorganic P for
560 each test site (Table 5) as follows:
561
562 **Table 5.** Additional test sites data used for model parameterisation
563

| | AGP-01[a,b] | CAX[a,b] | SA3[a,b] | Gig. Pen.[c] | Hawaii K.[b,d] |
|---|---|---|---|---|---|
| $Leaf_{C:P}$ | 600 | 600 | 600 | 700 | 691.5 |
| $Root_{C:P}$ | 1000 | 1000 | 1000 | 1750 | 1100 |
| $Wood_{C:P}$ | 3000 | 3000 | 3000 | 5500 | 5937.5 |
| $Soil_{C:P}$ | 2000 | 2000 | 2000 | 800 | 2000 |
| $K_{or-max}$ | 0.001 | 0.001 | 0.001 | 0.0033 | 0.001 |
| $K_{in-max}$ | 0.001 | 0.001 | 0.001 | 0.0185 | 0.001 |

564 [a]C:P ratios from Wang, Law and Pak, 2010 and [b]maximum sorbed P capacities from Yang *et al.*, 2014.
565 [c]Mirabello *et al.*, 2013 [d] C:P ratios from Vitousek, 2004
566
567 Model evaluation at test sites, was performed using observed NPP, litterfall, autotropic respiration, biomass and
568 soil C pools taken from different sources. We used NPP and litterfall for the Amazon sites from Aragão *et al.*,
569 (2009) and for Gigante Peninsula from Chave *et al.*, (2003), Hawaii Kokee NPP as reported in Goll *et al.*,
570 (2017) and litterfall as reported in (Yang *et al.*, 2014). Plant respiration was only available at two of Amazon
571 sites (AGP and CAX) (Malhi *et al.*, 2009). The biomass and soil C pools for Amazon sites (CAX and SA3) are
572 taken from  Malhi *et al.*, (2009) and biomass from AGP is taken from Jiménez *et al.*, (2009). The Gigante
573 Peninsula biomass is taken from Chave *et al.*, (2003), soil C from Turner et al., (2015), and the Hawaii Kokee C
574 pools are taking as reported in Yang et al., (2014).
575
576
577
578    **2.5  JULES simulations**
579
580 JULES was first applied at the K34 flux tower site using observed meteorological forcing data from 1999-2019
581 (Fleisher et a 2019) at half hourly resolution. The following meteorological variables are needed to drive JULES
582 (model inputs) (Best *et al.*, 2011): atmospheric specific humidity (kg kg$^{-1}$), atmospheric temperature (K), air
583 pressure at the surface (Pa), short and longwave radiation at the surface (W m$^{-2}$), wind speed (m s$^{-1}$) and total
584 precipitation (kg m$^{-2}$ s$^{-1}$). Furthermore, the averaged measured LAI from study site was used to initialise the
585 vegetation phenology module, but was allowed to vary in subsequent prognostic calculations. Soil organic and
586 inorganic sorbed P pools were initialised with study site observations. The JULES-CNP simulations were
587 initialized following the same methodology as in Fleischer et al., (2019), by the spin-up from1850 resulted in
588 equilibrium state (Figure S1). The spin up was performed separately for three versions of JULES (C/CN/CNP)
589 following the same procedure. Furthermore, the transient run was performed for the period 1851-1998 using
590 time-varying $CO_2$ and N deposition fields. Finally, for the extended simulation period (1999-2019) two runs
591 were performed, the first with ambient the second elevated $CO_2$ concentrations.
592
593 We evaluate the impact of including a P cycle in JULES using three model configurations (JULES C, CN and
594 CNP). We apply JULES in all three configurations using present day climate under both ambient $CO_2$ and $eCO_2$.
595 Ambient and $eCO_2$ were prescribed following Fleischer *et al.*, (2019), with present-day $CO_2$ based on global
596 monitoring stations, and an abrupt (step) increase in atmospheric $CO_2$ of +200 ppm on the onset of the transient
597 period (i.e., 1999). However, the comparison period is limited to 2017-18 for which the P measurements are
598 available.
599 We compare simulated C fluxes (GPP, NPP, litterfall C), C stocks (total vegetation, fine root, leaf, wood, soil)
600 and the $CO_2$ fertilization effect across model configurations. The $CO_2$ fertilization effect $\left(CO2_{fert-eff}\right)$ (eq.51)
601 is calculated based on simulated vegetation C under ambient $\left(VegC\left(aCO_2\right)\right)$ and $eCO_2$ $\left(VegC\left(eCO_2\right)\right)$ as
602 follows:
603
604 $CO2_{fert-eff} = \frac{\left(VegC\left(eCO_2\right)-VegC\left(aCO_2\right)\right)\times 100}{VegC\left(aCO_2\right)}$                                    (eq.51)
605
606

607 Furthermore, the net biomass increases due to CO$_2$ fertilization effect ($\Delta Cveg$) is estimated as follows:
608
609 $\Delta C_{veg} = \Delta BP - \Delta litterfall\ C$ (eq.52)
610
611 We studied the Water Use Efficiency (WUE) (eq. 53) at half-hourly timestep, then aggregated per month as one
612 of the main indicators of GPP changes (Xiao *et al.*, 2013), and soil moisture content (SMCL), as one of the
613 main controllers of maximum uptake capacity (eq. 27), in order to better understanding the changes in GPP, P
614 demand and uptake as well as excess C fluxes.
615
616 $WUE = GPP/Transpiration$ (eq.53)
617
618 Moreover, we also estimated the Carbon Use Efficiency (CUE) as an indicator of the required C for the growth
619 (Bradford and Crowther, 2013) as follows:
620
621 $CUE = BP/GPP$ (eq.54)
622
623 We use JULES-CNP to evaluate the extent of P limitation under ambient and eCO$_2$ at this rainforest site in
624 Central Amazon. P limitation is represented by the amount of C that is not used to grow new plant tissue due to
625 insufficient P in the system (excess C) (eq. 27). The excess C flux is highly dependent on the plant P and the
626 overall P availability to satisfy demand. We also explore the distribution of the inorganic and organic soil P and
627 their sorbed fraction within the soil layers and under ambient and eCO$_2$.
628
629 **2.5.1 Model sensitivity**
630
631 To test the sensitivity of the P and C related processes to individual model P parameters, six sets of simulations
632 were conducted independently with modified plant C:P stoichiometry (Plant C:P: *SENS1*), P uptake scaling
633 factor (K$_P$) (Kp: *SENS2*), inorganic (KP_sorb_in: *SENS3*) and organic (KP_sorb_or: *SENS4*) P adsorption
634 coefficients (K$_{sorb-or}$, K$_{sorb-in}$), and maximum inorganic (KP_sorb_in_max: *SENS5*) and organic
635 (KP_sorb_or_max: *SENS6*) sorbed P (K$_{or-max}$, K$_{in-max}$). These values were prescribed to vary between ±50%
636 of the observed values and their effect on C pools (plant and soil C) and fluxes (NPP and excess C), and P pools
637 (plant, soil, and soil sorbed P) was assessed. As the derived model parameters from measurements have their
638 own level of uncertainty, we took 50% change to test these parameters at reasonable degree. However, the
639 occluded and weathered P pools are prescribed for this model application, the occluded and weather P
640 coefficients (other two P-related model parameters) were not part of sensitivity tests.
641
642 Our model evaluation period is limited to years 2017-18 due to the P measurement availability. However, in
643 order to compare with 15 models studied by Fleischer *et al.*, (2019) we also studied the response of GPP, NPP
644 and BP to eCO$_2$ for both initial (1999) and 15 years periods (between 1999-2013).
645
646
647 **2.5.1    Simulations at test sites**
648
649 To perform JULES (C, CN, CNP) simulations at test sites we extracted the meteorological input data to drive
650 the model from a global dataset (CRU-NCEP)(Harris *et al.*, 2014) by selecting the closest grid cell to each site
651 when data were not available for a given site (Table 3). Soil texture ancillaries for each site were extracted from
652 a global soil data (HWSD) (Nachtergaele *et al.*, 2010). All simulations were initialised from a global JULES-CN
653 run (Wiltshire *et al.*, 2020) extracted for each site and further spun-up for 2000 years over the 1980-2000 period
654 for the three versions of JULES (C/CN/CNP). Finally, the transient (2000-2013) run was performed using the
655 output of the spin-up for each site.
656
657
658
659
660
661
662
663

## 3. Results

### 3.1 Model application under ambient CO$_2$

#### 3.1.1 Calibration of simulated soil P pools at *study site*

The maximum sorption capacities ($P_{in-max_n}$, $P_{or-max_n}$, eq.37 and 40) were calibrated to the observed P pools. As a result, JULES-CNP could reproduce the measured soil P pools (Fig. 2 and Table 6). Simulated inorganic soil P and sorbed organic and inorganic soil P closely matched the observations (Table 7 and Fig. 2). However, simulated organic soil P overestimates the observations by 60 %.
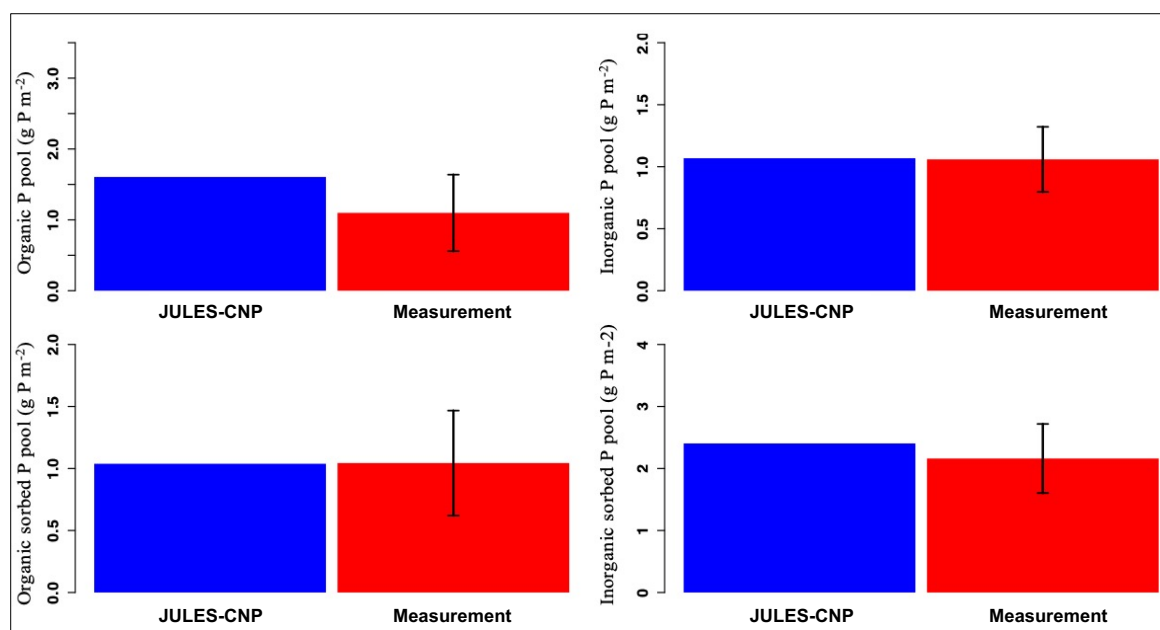
**Figure. 2-** Modelled vs measured soil phosphorus pools under ambient CO$_2$ (for the soil depth of 0-30cm). Black line represents standard deviation

**Table 6.** Observed and simulated phosphorus pools and fluxes. Occluded and weathered P pools were prescribed using the observed values (between period 2017-18).

| | Phosphorus pools and fluxes | | |
|---|---|---|---|
| | **Measured** | **Modelled Ambient CO$_2$** | **Modelled Elevated CO$_2$** |
| **Organic P** (g P m$^{-2}$) | 1.09±0.53 | 1.6 | 1.57 |
| **Inorganic P** (g P m$^{-2}$) | 1.05±0.33 | 1.07 | 0.96 |
| **Sorbed organic P** (g P m$^{-2}$) | 1.04±0.42 | 1.04 | 1.03 |
| **Sorbed inorganic P** (g P m$^{-2}$) | 2.1±0.55 | 2.4 | 2.4 |
| **Occluded P** (g P m$^{-2}$) | 7.98±2.38 | prescribed | prescribed |
| **Weathered P** (g P m$^{-2}$) | 0.59±12 | prescribed | prescribed |
| **Total vegetation P** (g P m$^{-2}$) | 4.15 | 4.66 | 5.11 |
| **Soil P** – 30cm (g P m$^{-2}$) | 13.85 | 14.7 | 14.56 |
| **Total ecosystem P** (g P m$^{-2}$) | - | 35.97 | 35.97 |
| **P litter flux** (g P m$^{-2}$yr$^{-1}$) | 0.3 | 0.28 | 0.29 |

687    **3.1.2    Model evaluation**

689 JULES-CNP could reproduce the plant and soil C (Figure 2 and Table 7) and N pools and fluxes (Figure S6 and
690 Table 8) under ambient $CO_2$. Our results show that simulated GPP, is within the range of measurement (3.02 kg
691 C $m^{-2}$ $yr^{-1}$ model vs 3-3.5 kg C $m^{-2}$ $yr^{-1}$ observed, respectively, Table 7).

693 Simulated NPP, is close to the measured values (NPP: 1.14 - 1.31 observed vs 1.26 modelled kg C $m^{-2}$ $yr^{-1}$) with
694 autotropic respiration (RESP) also closely following the observations (1.98 observed vs 1.81 modelled kg C $m^{-2}$
695 $yr^{-1}$). Biomass production is estimated as a difference between NPP and the amount of C which is not fixed by
696 plants due to the insufficient P in the system (excess C) (eq. 27). The excess C flux depends on the plant P and
697 the overall P availability to satisfy demand (Table 7). The simulated flux of excess C is 0.3 kg C $m^{-2}$ $yr^{-1}$ under
698 ambient $CO_2$. In JULES-CNP this flux is subtracted from NPP in order to give the BP (eq. 17) (Table 7). Our
699 simulated litterfall overestimates the observations by 32%, however simulated vegetation and its components
700 (fine root, leaf and wood) and soil C stocks match well the observations (Table 7).

702 **Table 7.** Observed and simulated carbon pools and fluxes with JULES-CNP (between period 2017-18)

| Carbon pools and fluxes | | | |
|---|---|---|---|
| | **Measured** | **Modelled Ambient $CO_2$** | **Modelled Elevated $CO_2$** |
| **GPP** (kg C $m^{-2}$ $yr^{-1}$) | 3.0 – 3.5 | 3.06 | 3.9 |
| **NPP$_{pot}$** (kg C $m^{-2}$ $yr^{-1}$) | - | 1.27 | 1.77 |
| **Plant respiration** (kg C $m^{-2}$ $yr^{-1}$) | 1.98 | 1.78 | 2.12 |
| **Excess C flux** (kg C $m^{-2}$ $yr^{-1}$) | - | 0.30 | 0.81 |
| **Biomass Production** (kg C $m^{-2}$ $yr^{-1}$) | 1.14±0.12 | 0.96 | 0.94 |
| **Litter C flux** (kg C $m^{-2}$ $yr^{-1}$) | 0.69±0.15 | 0.91 | 0.83 |
| **Leaf C** (kg C $m^{-2}$) | 0.37±0.2 | 0.38 | 0.40 |
| **Wood C** (kg C $m^{-2}$) | 22.01 | 22.4 | 24.71 |
| **Root C** (kg C $m^{-2}$) | 0.37±0.2 | 0.38 | 0.40 |
| **Vegetation C** (kg C $m^{-2}$) | 22.75±0.3 | 23.16 | 25.52 |
| **Soil C stock** (kg C $m^{-2}$) | 12.7 | 13.2 | 12.71 |
| **LAI** ($m^2$ $m^{-2}$) | 5.6±0.36 | 5.77 | 6.12 |

704    **3.1.3    Comparison of JULES C, CN and CNP under ambient $CO_2$ at *study site***

706 We compare simulated C pools and fluxes from JULES-C, JULES-CN and JULES-CNP (Figure 3). There is no
707 difference between C stocks and fluxes in simulations from JULES C and CN indicating that there is no N
708 limitation at this tropical site in the CN simulations. However, simulated BP and litter flux of C by JULES
709 C/CN are higher than in JULES-CNP but also overestimate the observations (litter flux of JULES C/CN: 1.18,
710 JULES-CNP: 0.91 and obs 0.69 (kg C $m^{-2}$ $yr^{-1}$) and BP of JULES C/CN: 1.24, JULES-CNP: 0.96 and obs 1.14-
711 1.31 (kg C $m^{-2}$ $yr^{-1}$), respectively). By including P cycling in JULES an excess C flux of 0.3 (kg C $m^{-2}$ $yr^{-1}$) is
712 simulated, indicating a 24% P limitation to BP at this site according to JULES-CNP, which represents a 29%
713 decrease in BP compared to JULES-C/CN. Consequently, the total vegetation C stock for models without P
714 inclusion is higher than the CNP version (+3% difference) due to the lack of representation of P limitation. The
715 simulated soil C stock in JULES C and JULES CN is also higher than in the CNP version (JULES C/CN: 13.93
716 vs. JULES-CNP: 13.18 (kg C $m^{-2}$ $yr^{-1}$)) and higher than the observations. Moreover, CUE in JULES C/CN
717 (eq.54) is higher than observations and JULES-CNP (JULES C/CN: 0.38 vs. JULES-CNP: 0.31, obs: 0.34
718 ±0.1(dimensionless).
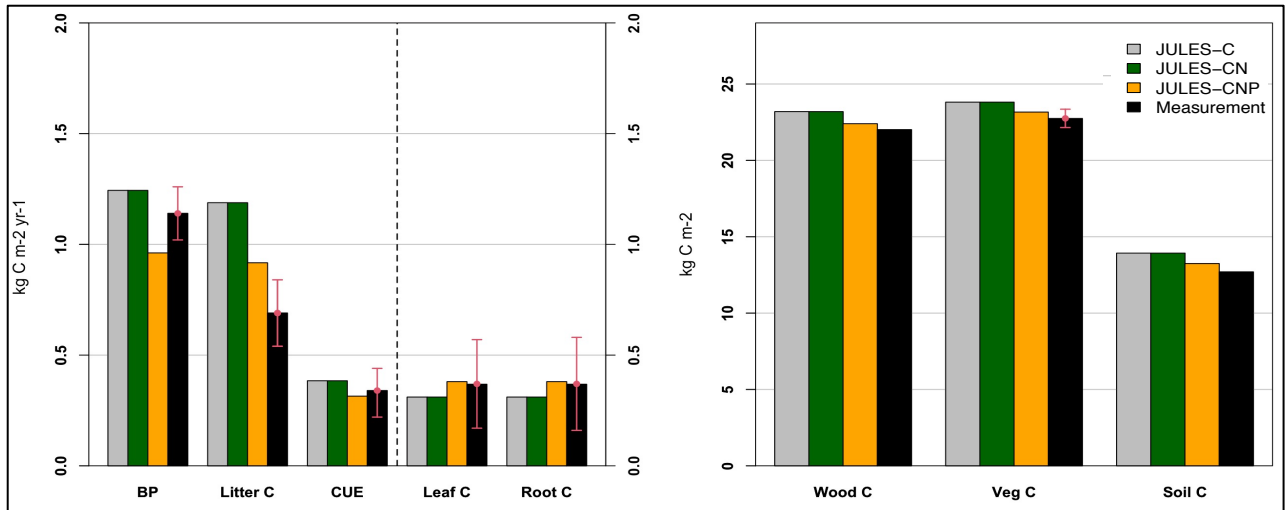
**Figure. 3-** JULES C, CN, CNP modelled vs measured C pools (Leaf, root, wood, Veg and Soil C) (in kg C m$^{-2}$) and fluxes (BP and Litter C) (in kg C m$^{-2}$ yr$^{-1}$) and CUE under ambient $CO_2$. Note that CUE is unitless.

### 3.1.4 Model evaluation at test sites under ambient $CO_2$

Evaluation of JULES C, CN and CNP at five test sites against the observed C pools and fluxes demonstrate that the inclusion of P processes improved the simulation of C pools and fluxes across all test sites (Figure 4). At all Amazon sites JULES C and CN overestimated BP compared to JULES-CNP which estimated lower BP values which were closer to the measurements for AGP (JULES-C: +35%, JULES-CN: +33%; JULES-CNP: +21%), CAX (JULES-C: +45%, JULES-CN: +44%; JULES-CNP: +7%) and SA3 (JULES-C: +27%, JULES-CN: +26%; JULES-CNP: -23%). Moreover, at Gigante Peninsula the C and CN versions overestimated BP (+42% and +40%, respectively), and CNP slightly underestimated BP (-15%). Furthermore, at the Hawaii Kokee site, all three versions of JULES underestimated the BP (C:-8%, CN:-8%, CNP: -32%). The litterfall and respiration fluxes in JULES-CNP have decreased compared to the JULES C and CN versions which overestimated both fluxes at all the test sites compared to the measurements. The litterfall flux comparisons show a significant overestimation using JULES C and CN versions across all the tested sites. Along the Amazon sites inclusion of P limitation reduced the litterfall flux but still overestimated (AGP: +50%, CAX: +24% and SA3: +16%) and at Gigante Peninsula and Hawaii Kokee slightly underestimated (Gigane Peninsula: -9% and Hawaii Kokee -19%). The respiration measurements were only available at two Amazon sites (CAX and SA3) at which inclusion of P limitation resulted in a well estimated flux at both sites compared to the JULES C/CN versions (CAX site: C-only: +38%, CN: +38%, CNP: -1%; SA3 site: C-only: +38%, CN: +38%, CNP: -2%). The total vegetation biomass also reduced using JULES-CNP compared to the other versions and yield closer values to the measurements across all the sites. However, except at the AGP site in which all three versions of JULES slightly underestimated the biomass (C: -1%, CN: -1%, CNP: -6%), at the other test sites JULES-CNP estimated lower biomass pools compared to the other versions which overestimated total vegetation biomass. Similarly, the soil C pool was overestimated prior to P limitation inclusion in JULES at the test sites, and the JULES-CNP estimated a closer value compared to the measurements (slight underestimation at CAX and SA3 sites: -5% and -18% respectively, and close values at Gigante Peninsula and Hawaii Kokee: +3% and +4%, respectively).
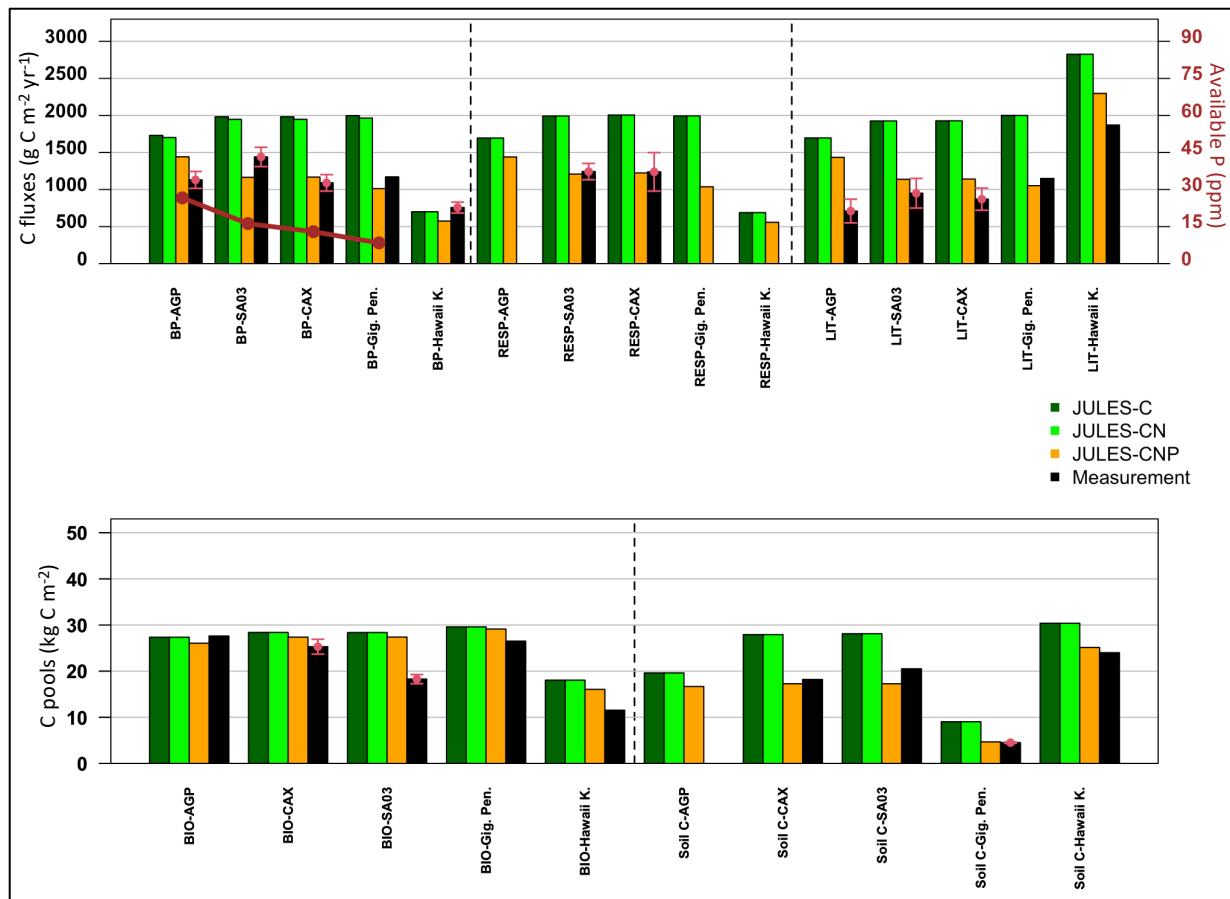
**Figure. 4-** Observed and simulated (JULES C, CN, CNP) C fluxes and pools (averaged measurements: red points, sd: red arrows) and available observed P (dark red points and lines (reported in ppm)) at test sites across the Amazon (AGP, SA03, CAX), Gigante Peninsula (Gig. Pen.) and Hawaii Kokee (Hawaii K.).

### 3.1.5 Model sensitivity

The results indicate that among all the corresponding C and P pools and fluxes, the excess C flux – which demonstrates P limitation to growth – shows the highest sensitivity to changes in C:P ratios (Figure 5-a), $K_P$ (Figure 5-b), and $K_{or-max}$ (Figure 5-c) and $K_{in-max}$ (Figure 5-d). A decrease in plant C:P results in a large increase in excess C. This is due to the higher plant P demand as a result of lower plant C:P ratios. An increase in the uptake factor and maximum sorbed organic and inorganic P also results in an increase in excess C. This is due to the higher uptake demand through higher uptake capacity (due to higher $K_P$) and lower available P for uptake due to higher organic and inorganic sorbed P (due to higher $K_{or-max}$, $K_{in-max}$). Since the total P in the system is lower than the plant demand, the uptake capacity and sorbed P, higher P limitation is placed on growth (decreasing BP) which results in an increase in excess C and decrease in plant C, but also soil C which is a result of lower litter input (Figure 5). Total soil P shows low sensitivity to changes in plant C:P and uptake factor but high sensitivity to maximum inorganic sorbed P. Moreover, sorbed P shows middle to high sensitivity to maximum organic and inorganic sorbed P respectively (Figure. S5). Nevertheless, organic and inorganic P adsorption coefficients ($K_{sorp-or}$, $K_{sorp-in}$) show no sensitivity to C and P pools and fluxes. This is due to limiting the organic and inorganic P sorption terms to be controlled only by maximum sorption capacity, hence no effect applied by organic and inorganic adsorption coefficients.
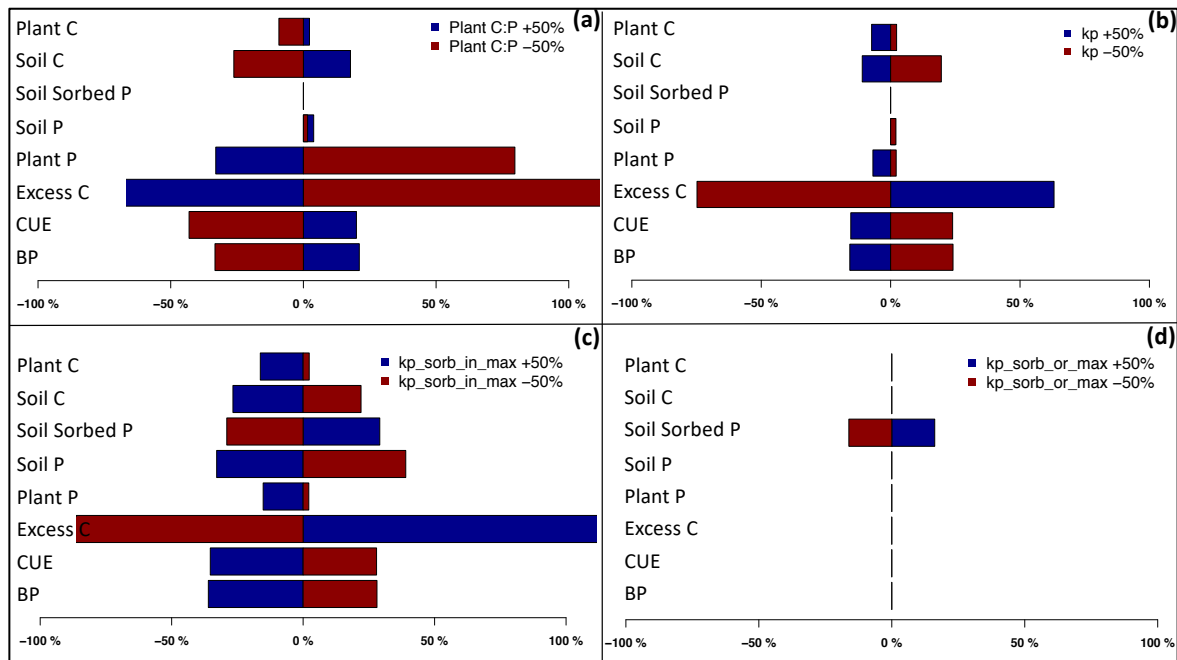
**Figure. 5-** Sensitivity of C and P pools to variation in key model parameters: prescribed tissue C:P (a), Kp(b), Kp_sorb_in(c), Kp_sorb_or(d) under ambient $CO_2$.

### 3.2 Model application under elevated $CO_2$

#### 3.2.1 Simulated plant and soil C and P pools and fluxes -JULES-CNP: e$CO_2$ vs ambient $CO_2$

The e$CO_2$ simulation using JULES-CNP yields a higher GPP compared to the ambient $CO_2$ (0.83 (kg C m$^{-2}$ yr$^{-1}$) increase), as a result of $CO_2$ fertilization. Moreover, due to the GPP increase, NPP and RESP also increased compared to ambient $CO_2$ (NPP: 0.49 and RESP:0.3 (kg C m$^{-2}$ yr$^{-1}$) increase) (Table 7). The total simulated vegetation C pool increases under e$CO_2$ compared to ambient $CO_2$ (0.41 kg C m$^{-2}$), hence the estimated plant P (estimated as a fraction of C:P ratios) increases as well (+0.45 (g P m$^{-2}$)) (Fig. 6, Table 6). Thus, the simulated plant P demand is higher, and as the total available soil P for uptake is limited, the simulated excess C flux increases to 0.51(kg C m$^{-2}$ yr$^{-1}$). Moreover, despite the higher NPP under e$CO_2$ compared to simulated NPP under ambient $CO_2$, due to the substantial increase in simulated excess C, the BP is similar to the ambient $CO_2$ (2% difference).

The simulated organic soil P under e$CO_2$ were close to those under ambient $CO_2$ (1.6 g P m$^{-2}$) (Table 7). This is due to the same parameterization of the output fluxes from this pool for e$CO_2$ and ambient $CO_2$. The simulated pool of inorganic P under e$CO_2$ decreases compared to the ambient $CO_2$ by 0.11 (g P m$^{-2}$) due to the increased plant P pools and slight increase in uptake (+0.13 %).
However, the simulated sorbed organic and inorganic soil P from e$CO_2$ are similar to those simulated under the ambient $CO_2$ which is due to the same parameterization of sorption function (maximum sorption capacity) from the ambient $CO_2$ run as explained in calibration section. Moreover, the modelled occluded and weathered soil P were similar to those in the ambient $CO_2$ simulation (Table 7) which is due to the same prescribed observational data that was used for this simulation.

#### 3.2.2 Comparison of JULES C, CN and CNP under elevated $CO_2$

JULES C/CN show higher vegetation and soil C pools, BP and litter flux compared to JULES-CNP: (Table 8, Figure. S2). Under e$CO_2$, simulated NPP using JULES C-CN is 4.5% higher than JULES-CNP and the BP with JULES- C/CN is 96.8% higher than in JULES-CNP which simulates an excess C flux of 0.81 (kg C m$^{-2}$ yr$^{-1}$) equivalent to 46% P limitation under e$CO_2$. As a result of P limitation and e$CO_2$, the simulated $CO_2$ fertilization effect estimated based on changes in biomass under ambient and e$CO_2$ was reduced from 13% with JULES-C/CN to 10% JULES-CNP. Moreover, the CUE from JULES C/CN is 87.5% higher than the JULES-CNP as a result of high P limitation over biomass production.

**Table 8.** Simulated C pools and fluxes with JULES C/CN and difference in percentage with JULES-CNP model under
eCO₂. A positive % means larger respective values simulated with JULES C and JULES CN than with JULES-CNP
(between period 2017-18).

|  | GPP | NPP | BP | CUE | Litter C | Leaf C | Root C | Wood C | Soil C |
|---|---|---|---|---|---|---|---|---|---|
| **JULES C/CN** | 4.1 | 1.85 | 1.85 | 45% | 1.77 | 0.42 | 0.42 | 26.1 | 19.2 |
| **JULES-CNP** | 3.9 | 1.77 | 0.94 | 24% | 0.83 | 0.4 | 0.4 | 24.71 | 12.71 |
| **ΔC/CN: CNP** | 5.1% | 4.5% | 96.8% | 87.5% | 113.3% | 5% | 5% | 5% | 51.1% |

### 3.2.2.1 Inter-models under elevated CO₂

Following Fleischer *et al.*, (2019), we report the simulated response to eCO₂ for year 1999 (initial: CO₂ effect)
and 1999-2013 (15 years: final effect) which are different than our evaluation period (2017-18). Using JULES-C
and JULES-CN under eCO₂, simulated GPP and NPP during the 1st year increase by 30% and 61% respectively
and by 28% and 52% after 15 years (Figure. 6). However, using JULES-CNP, eCO₂ increases simulated GPP,
NPP and BP responses during the 1st year by 29%, 51% and 20% and by 28%, 43% and 7%, after 15 years,
respectively.

Corresponding simulated CUE during the 1st year and 15 years shows an increase of 24% and 20% in response
to eCO₂ using JULES C/CN, respectively. However, using JULES-CNP, simulated CUE for the 1st and after 15
years is reduced by 7% and17% in response to eCO₂.

Simulated total biomass (leaf, fine root and wood C) (ΔCveg) using JULES- C/CN for the 1st and 15 years of
eCO₂ increased by 9% and 13% respectively. However, using JULES-CNP ΔCveg only increases by 0.5% and
9% for 1st and 15 years of eCO₂, respectively.
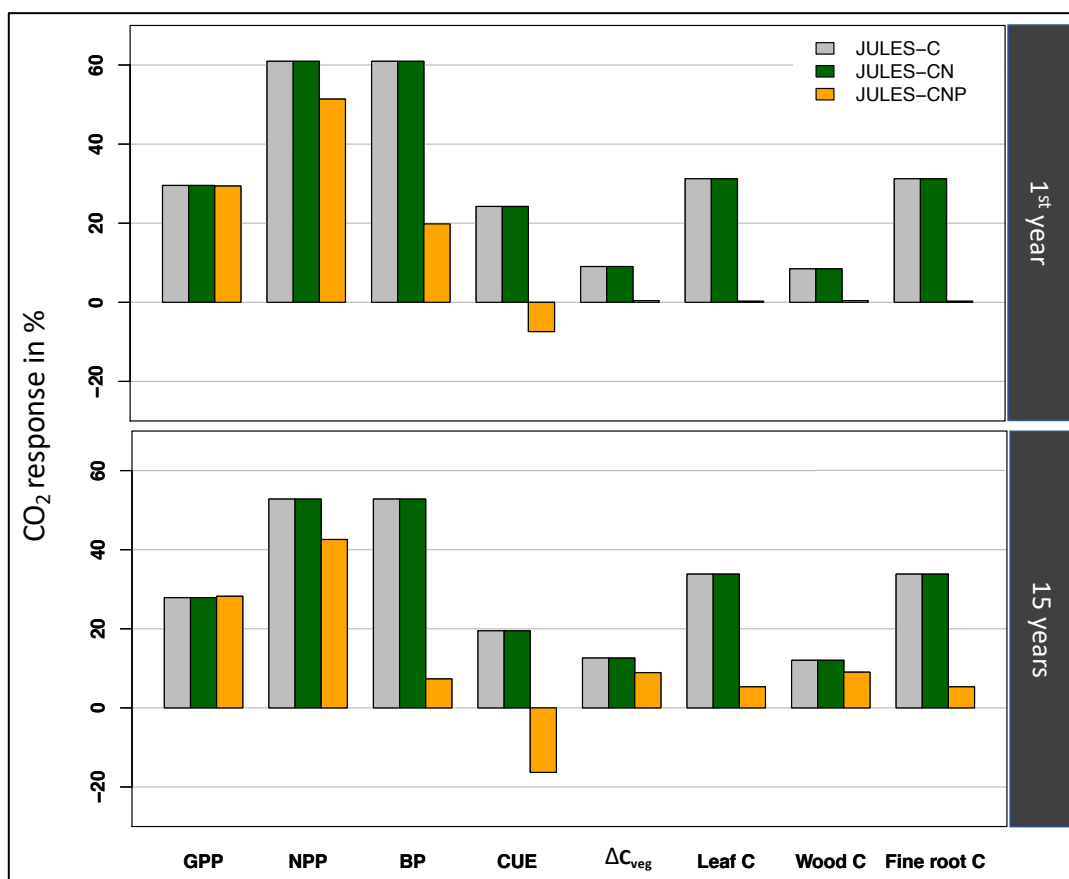
**Figure. 6-** Relative effect of eCO₂ on simulated GPP, NPP, BP, CUE, ΔC*veg*, leaf C, wood C and fine root C, using three
versions of JULES model in 1st (initial response) and 15 years periods (final response).

### 3.3 Plant P Demand, uptake and excess C under ambient and elevated CO₂

To understand further the CP-cycle dynamics, we studied the monthly averaged plant P demand and the relative (limited) P uptake (eq. 26) under both ambient and elevated $CO_2$ conditions (Figure. 7).

Under ambient $CO_2$ condition the highest GPP is estimated at $0.29\pm0.016$ kg C m$^{-2}$ month$^{-1}$ in July and the lowest at $0.17\pm0.051$ kg C m$^{-2}$ month$^{-1}$ in October (Figure. 7-a). The estimated WUE and SMCL in October is among the lowest estimated monthly values at $2.3\pm0.51$ kg $CO_2$/kg $H_2O$ and $526.2\pm31$ kg m$^{-2}$ respectively (Figure. 7-c). The highest P demand is estimated at $0.4\pm0.02$ g P m$^{-2}$ month$^{-1}$ in July and the lowest demand at $0.2\pm0.08$ g P m$^{-2}$ month$^{-1}$ in October. Consequently, the highest and lowest uptake ($0.32\pm0.01$ and $0.19\pm0.07$ g P m$^{-2}$ month$^{-1}$, respectively). The excess C for the highest and lowest GPP and demand periods are estimated at $0.4\pm15$ and $0.04\pm0.07$ kg C m$^{-2}$ month$^{-1}$, respectively.

However, similar to ambient $CO_2$, under $eCO_2$ condition the highest estimated GPP is in July at $0.36\pm0.017$ kg C m$^{-2}$ month$^{-1}$ and lowest for October $0.25\pm0.062$ kg C m$^{-2}$ month$^{-1}$ (Figure. 7-b). The estimated WUE and soil moisture content (SMCL) for the lowest GPP period is among the lowest monthly estimated values at $3.5\pm0.74$ kg $CO_2$/kg $H_2O$ and $552\pm33$ kg m$^{-2}$ for October respectively (Figure. 7-d). The highest P demand is estimated for July at $0.51\pm0.02$ g P m$^{-2}$ month$^{-1}$ with the uptake flux of $0.31\pm0.02$ g P m$^{-2}$ month$^{-1}$ and the lowest demand is estimated for October at $0.32\pm0.1$ g P m$^{-2}$ month$^{-1}$ with the estimated uptake flux of $0.26\pm0.06$ g P m$^{-2}$ month$^{-1}$. The highest excess C flux is also for July at $1.01\pm0.17$ kg C m$^{-2}$ month$^{-1}$ and lowest for October $0.27\pm0.29$ kg C m$^{-2}$ month$^{-1}$, respectively.

However, despite the P limitation in both $eCO_2$ and ambient $CO_2$ conditions, the P uptake flux under $eCO_2$ is higher than the ambient $CO_2$ condition. This is due to the higher WUE and increased SMCL (controlling uptake capacity (eq. 27)) under $eCO_2$ condition, hence more water availability during the dry season to maintain productivity and critically transport P to the plant (see eq. 27), compared to ambient $CO_2$ condition (Figure. 7-c and d). Additionally, in JULES both the vertical discretisation (Burke, Chadburn and Ekici, 2017) and mineralisation terms (Wiltshire *et al.*, 2021) depend on the soil moisture and temperature. Thus, higher P concentration and uptake under $eCO_2$ condition.
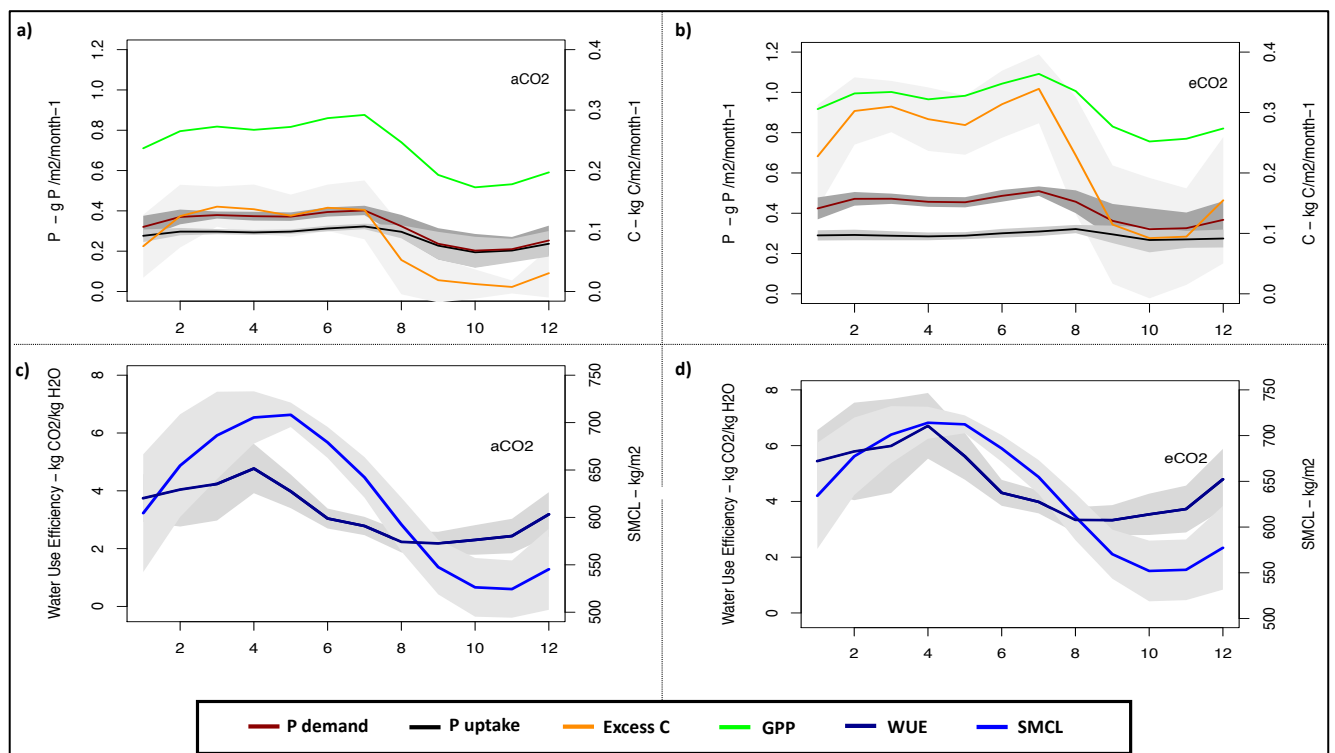
**Figure. 7-** Simulated monthly plant P demand and uptake (g P m$^{-2}$ month$^{-1}$), excess C and GPP (kg C m$^{-2}$ month$^{-1}$) under a) $aCO_2$ and b) $eCO_2$, water use efficiency (g m$^{-2}$ month$^{-1}$) under c) ambient $CO_2$ ($aCO_2$) and d) $eCO_2$ conditions. The grey area represents the standard deviation.

### 3.4 Soil P pools profile under ambient $CO_2$ and elevated $CO_2$

We explored the distribution of the inorganic and organic soil P and their sorbed fraction within the soil layers and under different $CO_2$ conditions (Figure. S3). Both the ambient and $eCO_2$ simulations have a close inorganic soil P distribution at the topsoil layer (0-30cm) (0.85 vs. 0.9 (g P m$^{-2}$) respectively) as well as similar organic soil P distribution (0.85 vs 0.9 (g P m$^{-2}$) respectively).

However, the organic soil P and sorbed forms of inorganic and organic soil P profiles are not changing significantly between different sets due to the similar parameterization of the processes that control these pools (processes which are related to the physical aspects of soils, hence not changing under $eCO_2$ condition) and the same parameter values used for both ambient and $eCO_2$ runs.

Moreover, the soil P within 30cm soil depth for ambient and $eCO_2$ conditions is at 14.7 (g P m$^{-2}$) and 14.56 (g P m$^{-2}$) respectively, and the total ecosystem P for both ambient and $eCO_2$ conditions is at 35.97 (g P m$^{-2}$). However, the slightly lower soil P in the $eCO_2$ condition is due to the higher plant P demand compared to the ambient condition, hence the higher allocated P vegetation (10%) under $eCO_2$ condition.

## 4. Discussion

Studies show the significant role of the tropical forests, and Amazonia in particular, in C uptake and regulating atmospheric $CO_2$ (Brienen *et al.*, 2015; Phillips *et al.*, 2017). As soil P availability is low in the majority of Amazonia (Quesada *et al.*, 2012), the competition for nutrients by both plant and soil communities is high (Lloyd *et al.*, 2001). The responses of these communities to $eCO_2$ under P limited conditions remains uncertain (Fleischer *et al.*, 2019). These responses in P enabled models are represented in different ways regarding the excess C which is not used for plant growth due to P limitation. Either growth is directly downregulated taking the minimum labile plant C, N and P (Goll *et al.*, 2017), or photosynthesis is downregulated via $V_{cmax}$ and $J_{max}$ (Comins and McMurtrie, 1993; Yang *et al.*, 2014; Zhu *et al.*, 2016) and models like JULES-CNP downregulate NPP via respiration of excess carbon that cannot be used for growth due to plant nutrient constraints (Haverd *et al.*, 2018). The estimated CUE depends on the modelling approach. Models that down regulate the photosynthetic capacity and GPP consequently (Comins and McMurtrie, 1993; Yang *et al.*, 2014; Zhu *et al.*, 2016) simulate a positive CUE response to $CO_2$ fertilization while models that down regulate the NPP and respire the excess C (Haverd *et al.*, 2018) simulate a negative CUE response (Fleischer *et al.*, 2019) which is in line with field studies showing lower CUE when nutrient availability declines (Vicca *et al.*, 2012b). However, this remains a major uncertainty in understanding the implication of P limitation on terrestrial biogeochemical cycles.
The JULES-CNP structure represent key P processes in both plant and soil pools and can be applied to the Amazon region using existing soil (Quesada *et al.*, 2011) and foliar structural and nutrient (Fyllas *et al.*, 2009) data for parameterisation. The model can be applied globally and under future climate projections using global soil P data (Sun *et al.*, 2021) for model initialization and PFT-specific plant (Zechmeister-Boltenstern et al. 2015) and soil stoichiometries (Zechmeister-Boltenstern et al. 2015; Tipping et al. (2016), sorption and weathering ratios (based on lithological class specific from the GliM lithological map (Hartmann and Moosdorf, 2012) and soil shielding from Hartmann et al., (2014)).

### 4.1. Evaluation of model performance

At the study site, JULES-CNP could reproduce the magnitude of soil organic and inorganic P pools and fluxes. The relative distribution of total organic P, total inorganic P and residue P fractions of total P in soils under Brazilian Eucalyptus plantations (Costa *et al.*, 2016) shows inorganic P fraction of 28% from total soil P which is close to our estimation of 24% and organic P fraction of 30% from total soil P which is higher than our estimated fraction of 18%. Thus, we may need to improve the process representation or parameters that control the organic P concentration, such as litter flux and decomposition, soil organic P mineralization, and immobilization in the future.

Our estimated maximum P uptake, which represents the actual available P for plant uptake (Goll *et al.*, 2017), for both ambient and $eCO_2$, is highly correlated with the plant P demand ($R^2 = 0.96$ and 0.52 respectively). The plant P demand depends on the GPP changes which are reflected by the WUE (Hatfield and Dold, 2019). Hence, under ambient $CO_2$, JULES-CNP simulates lower GPP and plant P demand during the dry season than during the wet season. Sufficient P uptake during these periods results in the lowest P limitation, thus the lowest simulated excess C. Nevertheless, under $eCO_2$ the same pattern is simulated but a higher availability of soil P due to the stomatal closure in the dry season. Hence, due to the plant's more efficient water usage, the soil

939 moisture in the dry season is higher (Xu *et al.*, 2016) which impacts our capped P uptake flux (eq. 27) and
940 increases the uptake capacity respectively.
941
942 Overall, JULES-CNP reproduced the observed C pools and fluxes which are in the acceptable ranges compared
943 to the measurements. However, using the JULES default $V_{cmax}$ estimation method (eq. 40), the model slightly
944 underestimates the total GPP (2.9 kg C m$^{-2}$ yr$^{-1}$ vs. 3-3.5 kg C m$^{-2}$ yr$^{-1}$). Therefore, in this version of the model,
945 we used the improved $V_{cmax}$ estimation method based on N and P (eq. 46) which resulted in a final estimated
946 GPP closer to the measurements (3.06 kg C m$^{-2}$ yr$^{-1}$).
947
948 Our results show an increase in GPP (21%) in response to eCO$_2$ which is higher than the average increase of
949 GPP reported in mature eucalyptus forests (11%), also growing under low P soils at the free air CO$_2$ enrichment
950 experiment (EucFACE) facility in Australia (Jiang *et al.*, 2020). This can be related to the lower decrease of
951 biomass growth response estimated by JULES-CNP (-3%) compared to the measurements from mature
952 eucalyptus forests (-8%) (Ellsworth *et al.*, 2017), due to the P limitation which was shown to impact the above-
953 ground biomass growth response in mature forests (Körner *et al.*, 2005; Ryan, 2013; Klein *et al.*, 2016).
954
955 In order to estimate the biomass production (BP), we deducted the excess C fluxes from NPP. Using JULES
956 C/CN models, the simulated biomass productivity enhancement due to eCO$_2$ (49%) is in the middle range of the
957 reported for different biomes by Walker *et al.*, (2021). Moreover, our estimated difference of BP between
958 ambient and eCO$_2$ conditions (2%) is close to the estimated difference for mature forests (3%) (Jiang *et al.*,
959 2020).
960
961 A global estimation for tropical forests using the CASA-CNP model which includes N and P limitations on
962 terrestrial C cycling, shows that NPP is reduced by 20% on average due to the insufficient P availability (Wang,
963 Law and Pak, 2010) which is close to our estimated P limitation of 24%. This finding is in line with a field study
964 that shows a strong correlation between the total NPP and the soil available P (Aragão *et al.*, 2009).
965 The estimated decrease of NPP in response to eCO$_2$ as a result of P limitation is in line with the findings from
966 CLM-CNP model at five tropical forests (Yang *et al.*, 2014) which indicates the CO$_2$ fertilization dependency
967 on the processes that affect P availability or uptake.
968
969 Our estimated CUE (0.31) is close to that by Jiang *et al.* (2020) for mature eucalyptus forests (0.31±0.03), as
970 well as to the measurement for our study site (0.34 ±0.1). There is currently a lack of representation of stand age
971 in JULES-CNP which can significantly affect CUE (e.g. mature trees are less responsive to the nutrient
972 limitations) (De Lucia *et al.*, 2007; Norby *et al.*, 2016). However, a recent development of Robust Ecosystem
973 Demography (RED) model in JULES (Argles *et al.*, 2020) and its integration into JULES-CNP in the future can
974 address this issue.
975
976 Under low P availability, all available P is considered to be adsorbed or taken by plant and microbes for further
977 consumption, with leaching considered to be minor within the time scales of our study period (Went and Stark,
978 1968; Bruijnzeel, 1991; Neff, Hobbie and Vitousek, 2000). Despite studies that show the possibility of P
979 fixation as a source of available P for plants (Van Langenhove *et al.*, 2020; Gross *et al.*, 2021), due to the strong
980 fixation of P in the soil (Aerts & Chapin, 2000; Goodale, Lajtha,Nadelhoffer, Boyer, & Jaworski, 2002), the P
981 deposited is unlikely to be available to plants in the short term (de Vries et al., 2014), for this reason this
982 version of JULES-CNP did not include P deposition. However both P deposition and leaching are likely to have
983 a very important role on sustaining the productivity of tropical forests in the Amazon over longer time scales
984 (Van Langenhove *et al.*, 2020) and needs to be considered in future studies. Moreover, biochemical
985 mineralisation is also not included in the current version of JULES-CNP which only accounts for total
986 mineralization. However, models that include this process show no significant difference between total and
987 biochemical mineralized P which can be due to complexity of identifying the inclination of mineralization
988 versus uptake (Martins *et al.*, 2021). Lastly, in order to capture plant internal nutrient impact on the C storage,
989 future work should focus on implementing recent developments including Non-Structural Carbohydrate pools
990 (NSC) (Jones *et al.*, 2020) in JULES-CNP.
991
992
993
994
995
996
997
998

### 4.1.1. Evaluation of model performance at test sites

Overall, inclusion of P processes in JULES-CNP improved the previously overestimated C fluxes and pools using JULES-C and -CN versions. Generally, the biomass productivity tends to follow the observed P availability (Figure 4), where the sites with higher available P for uptake simulated higher productivity which is in line with observations across P availability in the Amazon (Aragão *et al.*, 2009). Nevertheless, this tendency could be altered if the natural conditions in these forests are perturbated. For instance, in case of the high mortality events in these P limited sites (Malhi *et al.*, 2009; Pyle *et al.*, 2009), regrowing forests developing over the highly weathered oxisols with limited available P (Davidson *et al.*, 2004), results in the shifting limitation from P to N (Herbert, Williams and Rastetter, 2003). Hence, the controlling processes under N limitation will be N-related and processes such as N leaching or outgassing (Yang *et al.*, 2014) will define the productivity. This shifting in limitation condition is not represented by JULES-CNP, therefore at few tested sites the model overestimated the P limitation, thus underestimated the productivity below the measured values. Moreover, the higher (than other sites) BP in JULES C/CN at the the Gigante Peninsula is related to the higher solar radiation in the forcing data at this site (Figure S8).

The estimated litterfall and respiration fluxes were considerably lower with JULES-CNP than JULES-C and -CN due to the lower simulated NPP with the former in closer agreement with the observations at all sites. Consequently, the total vegetation and soil C pools have lower values under the P limitation (Malhi *et al.*, 2009), which could not be captured by JULES-C and -CN and successfully represented by JULES-CNP.

As shown in Figure 5, JULES-CNP is highly sensitive to the five parameters needed to run JULES-CNP in addition to JULES-C and JULES-CN which were prescribed for simulations at test sites. The successful model performance at these sites demonstrates the importance of these parameters in JULES-CNP with implications for global scale simulations.

## 4.2. Inter-models Comparison of JULES C, CN and CNP

The comparison of simulated GPP enhancement across JULES versions for the 1st year is within the middle range of the 1st year $CO_2$ responses of the C/CN models studied by Fleischer *et al.*, (2019) evaluating simulated $eCO_2$ effects at a site in Manaus using the same meteorological forcing and methodology used in this study for a range of DGVM's. However, comparison for 15 years of $eCO_2$, shows that the simulated response with JULES-CNP is on the higher end of Fleischer *et al.*, (2019) study which is due to the higher estimated biomass growth by JULES-CNP (Table S1). Similarly, using JULES-CNP our estimated GPP enhancement is on the higher end of model estimations in Fleischer *et al.*, (2019). Moreover, comparing the GPP responses between different versions of (JULES C/CN and CNP), the JULES-CNP shows a slightly higher response to $CO_2$ fertilization associated with the higher WUE changes (Xiao *et al.*, 2013) (Figure. S4). This is due to the higher sensitivity of the plant to water availability than P availability in the P limited system (He and Dijkstra, 2014). Hence, under $eCO_2$ due to water-saving strategy of plants and stomatal closure (Medlyn *et al.*, 2016), simulated transpiration is decreased (Sampaio *et al.*, 2021) and photosynthesis is enhanced compared ambient $CO_2$ .

To that end, the monthly changes of WUE in JULES-CNP are highly correlated to the GPP, hence the lowest and highest WUE follow the same periods as GPP similar to responses captured with models studied by Fleischer *et al.*, (2019) (Table. S1).

Our estimated NPP enhancement using JULES C/CN models for both 1st and 15 years period is within the middle range of the models in Fleischer *et al.*, (2019). Nevertheless, JULES-CNP response of BP is in the lower band of the CNP models in Fleischer *et al.*, (2019) and close to the estimations from CABLE (Haverd *et al.*, 2018) and ORCHIDEE (Goll *et al.*, 2017) models, which may be due to the similar representation of P processes and limitation between these models. However, our results show a 29% decrease in NPP using JULES-CNP compared to JULES-C/CN which is smaller than the differences between the CLM-CNP and CLM-CN versions (51% decrease) (Yang *et al.*, 2014). The lower estimated decrease in JULES highlights the need to further study the fully corresponding plant C pools and fluxes to the changes in soil and plant P. Therefore, future work should be focused on the improvement of the total P availability and the plant C feedbacks. Moreover, there are other environmental factors such as temperature which shows a possible impact on the $CO_2$ elevation and the changes of NPP (Baig *et al.*, 2015) which needs further improvement in our model.

The CUE estimations of 1st year and 15 years response to $CO_2$ elevation from JULES C/CN are in the middle range of C/CN models in Fleischer *et al.*, (2019). However, the estimated CUE using JULES-CNP for 1st and 15 years are in the low range of CNP models reported by Fleischer *et al.*, (2019) which is due to the same reason discussed for NPP comparison.

1059 Finally, our estimated total biomass enhancement ($\Delta C veg$) using JULES C/CN for the 1st and 15 years are in the
1060 middle range of C/CN models from Fleischer *et al.*, (2019) and in lower range of CNP models from Fleischer *et*
1061 *al.*, (2019) using JULES-CNP. Nevertheless, while JULES-CNP includes the trait-based parameters (Harper *et*
1062 *al.*, 2016), other functions such as flexible C allocation and spatial variation of biomass turnover are still
1063 missing and future model improvement should be focused on their inclusion.

1064
1065 **5. Conclusion**

1066
1067 Land ecosystems are a significant sink of atmospheric $CO_2$, ergo buffering the anthropogenic increase of this
1068 flux. While tropical forests contribute substantially to the global land C sink, observational studies show that a
1069 stalled increase in carbon gains over the recent decade (Brienen *et al.*, 2015; Hubau *et al.*, 2020). However
1070 modelling studies that lack representation of P cycling processes predict an increasing sink (Fernández-Martínez
1071 *et al.*, 2019; Fleischer *et al.*, 2019). This is particularly relevant for efforts to mitigate dangerous climate change
1072 and assumptions on the future efficacy of the land C sink. Therefore, in this study, we presented the full
1073 terrestrial P cycling and its feedback on the C cycle within the JULES framework. Our results show that the
1074 model is capable of representing plant and soil P pools and fluxes at a site in Central Amazon and across the
1075 extended P limited test sites in Amazon, Gigante Peninsula and Hawaii chronosequence provided with site level
1076 data for model parameterisation. Moreover, the model estimated a significant NPP limitation under ambient
1077 $CO_2$, due to the high P deficiency at these sites which is representative of Central Amazon and tropical P limited
1078 sites, and elevated $CO_2$ resulted in a further subsequent decrease in the land C sink capacity relative to the
1079 model without P limitation. While our study is a step toward the full nutrient cycling representation in ESMs, it
1080 can also help the empirical community to test different hypotheses (i.e., dynamic allocation and stoichiometry)
1081 and generate targeted experimental measurements (Medlyn *et al.*, 2015).

1082
1083 *Code availability*

1084 The modified version of JULES vn5_5 and the P extension developed for this paper are freely available on Met
1085 Office Science Repository Service:
1086 https://code.metoffice.gov.uk/svn/jules/main/branches/dev/mahdinakhavali/vn5.5_JULES_PM_NAKHAVALI/
1087 after registration (http://jules-lsm.github.io/access_req/JULES_access.html) and completion of software license
1088 form. Codes for compiling model available at: (https://doi.org/10.5281/zenodo.5711160). Simulations were
1089 conducted using two sets of model configurations (namelists): ambient $CO_2$ condition
1090 (https://doi.org/10.5281/zenodo.5711144) and elevated $CO_2$ condition
1091 (https://doi.org/10.5281/zenodo.5711150).

1092 *Data availability*

1093 The model outputs related to the results in this paper are provided on Zenodo repository
1094 (https://doi.org/10.5281/zenodo.5710898). All the R scripts used for processing the model outputs and
1095 producing results in form of table or figures are provided on Zenodo repository
1096 (https://doi.org/10.5281/zenodo.5710896).

1097 *Author contributions.* MAN, LMM, SS, SEC, CAQ, AJW, IAP, KMA and DBC developed the model, per-
1098 formed simulations and analysis. CAQ, FVC, RP, LFL, KMA, GR, LS, ACMM, JSR, RA and JLC provided the
1099 measurements for the model parasitisation and evaluation. MAN, LMM, SS, IAP, SEC, FVC, RP, LFL, KMA
1100 and DBC contributed in writing the manuscript.

1101
1102 *Competing interests.* The authors declare no competing interests

1103
1104 *Acknowledgment*s. This work and its contributors (MAN, LMM, KMA and IPH) were supported by the UK
1105 Natural Environment Research Council (NERC) grant no. NE/LE007223/1. MAN, LMM, SS, IPH were also
1106 supported by the Newton Fund through the Met Office Climate Science for Service Partnership Brazil (CSSP
1107 Brazil). LMM acknowledges support from the Natural Environment Research Council, grant NEC05816 LTS-
1108 M-UKESM. LFL was also supported by AmazonFACE programme (CAPES) and the National Institute of
1109 Amazonian Research, grant no: 88887.154643/2017-00. The authors acknowledge contributions from Celso
1110 Von Randow towards data curation of the meteorological forcing used in this study and Daniel Goll for
1111 modelling insight. We would like to thank Alessandro C. de Araújo and the Large-Scale Biosphere-Atmosphere
1112 Program (LBA), coordinated by the National Institute for Amazon Researches (INPA), for the use and
1113 availability of data.

**References:**

Aerts, R. and Chapin, F. S. (1999) 'The Mineral Nutrition of Wild Plants Revisited: A Re-evaluation of Processes and Patterns', *Advances in Ecological Research*, 30(C), pp. 1–67. doi: 10.1016/S0065-2504(08)60016-1.

Anav, A. *et al.* (2013) 'Evaluating the land and ocean components of the global carbon cycle in the CMIP5 earth system models', *Journal of Climate*, 26(18), pp. 6801–6843. doi: 10.1175/JCLI-D-12-00417.1.

Aragão, L. E. O. C. *et al.* (2009) 'Above- and below-ground net primary productivity across ten Amazonian forests on contrasting soils', *Biogeosciences Discussions*, 6(1), pp. 2441–2488. doi: 10.5194/bgd-6-2441-2009.

Aragõ, L. E. O. C. *et al.* (2009) 'Above- and below-ground net primary productivity across ten Amazonian forests on contrasting soils', *Biogeosciences*, 6(12), pp. 2759–2778. doi: 10.5194/bg-6-2759-2009.

Araújo, A. C. *et al.* (2002) 'Comparative measurements of carbon dioxide fluxes from two nearby towers in a central Amazonian rainforest: The Manaus LBA site', *Journal of Geophysical Research*, 107(D20), p. 8090. doi: 10.1029/2001JD000676.

Argles, A. P. K. *et al.* (2020) 'Robust Ecosystem Demography (RED version 1.0): A parsimonious approach to modelling vegetation dynamics in Earth system models', *Geoscientific Model Development*, 13(9), pp. 4067–4089. doi: 10.5194/gmd-13-4067-2020.

Arora, V. K. *et al.* (2020) 'Carbon–concentration and carbon–climate feedbacks in CMIP6 models and their comparison to CMIP5 models', *Biogeosciences*, 17(16), pp. 4173–4222. doi: 10.5194/bg-17-4173-2020.

Baig, S. *et al.* (2015) 'Does the growth response of woody plants to elevated CO2 increase with temperature? A model-oriented meta-analysis', *Global Change Biology*, 21(12), pp. 4303–4319. doi: 10.1111/gcb.12962.

Baker, T. R. *et al.* (2004) 'Variation in wood density determines spatial patterns in Amazonian forest biomass', *Global Change Biology*, 10(5), pp. 545–562. doi: 10.1111/j.1365-2486.2004.00751.x.

Bentsen, M. *et al.* (2013) 'The Norwegian Earth System Model, NorESM1-M – Part 1: Description and basic evaluation of the physical climate', *Geoscientific Model Development*, 6(3), pp. 687–720. doi: 10.5194/gmd-6-687-2013.

Best, M. J. *et al.* (2011) 'The Joint UK Land Environment Simulator (JULES), model description – Part 1: Carbon fluxes and vegetation dynamics', *Geoscientific Model Development*, 4(3), pp. 701–722. doi: 10.5194/gmd-4-701-2011.

Bradford, M. A. and Crowther, T. W. (2013) 'Carbon use efficiency and storage in terrestrial ecosystems', *New Phytologist*, 199(1), pp. 7–9. doi: 10.1111/nph.12334.

Brienen, R. J. W. *et al.* (2015) 'Long-term decline of the Amazon carbon sink', *Nature*, 519(7543), pp. 344–348. doi: 10.1038/nature14283.

Bruijnzeel, L. A. (1991) 'Nutrient input—output budgets of tropical forest ecosystems: A review', *Journal of Tropical Ecology*, 7(1), pp. 1–24. doi: 10.1017/S0266467400005010.

Burke, E. J., Chadburn, S. E. and Ekici, A. (2017) 'A vertical representation of soil carbon in the JULES land surface scheme (vn4.3-permafrost) with a focus on permafrost regions', *Geoscientific Model Development*, 10(2), pp. 959–975. doi: 10.5194/gmd-10-959-2017.

Castanho, A. D. A. *et al.* (2013) 'Improving simulated Amazon forest biomass and productivity by including spatial variation in biophysical parameters', *Biogeosciences*, 10(4), pp. 2255–2272. doi: 10.5194/bg-10-2255-2013.

Chapin, F. S. *et al.* (2011) *Principles of Terrestrial Ecosystem Ecology*. Springer New York (Biomedical and Life Sciences). Available at: https://books.google.co.uk/books?id=68nFNpceRmIC.

Chave, J. *et al.* (2003) 'Spatial and temporal variation of biomass in a tropical forest: Results from a large census plot in Panama', *Journal of Ecology*, 91(2), pp. 240–252. doi: 10.1046/j.1365-2745.2003.00757.x.

Chave, J. *et al.* (2014) 'Improved allometric models to estimate the aboveground biomass of tropical trees', *Global Change Biology*, 20(10), pp. 3177–3190. doi: 10.1111/gcb.12629.

Clark, D. B. *et al.* (2011) 'The Joint UK Land Environment Simulator (JULES), model description – Part 2: Carbon fluxes and vegetation dynamics', *Geoscientific Model Development*, 4(3), pp. 701–722. doi: 10.5194/gmd-4-701-2011.

Collatz, G. J. *et al.* (1991) 'Physiological and environmental regulation of stomatal conductance, photosynthesis and transpiration: a model that includes a laminar boundary layer', *Agricultural and Forest Meteorology*, 54(2–4), pp. 107–136. doi: 10.1016/0168-1923(91)90002-8.

Collatz, G., Ribas-Carbo, M. and Berry, J. (1992) 'Coupled Photosynthesis-Stomatal Conductance Model for Leaves of C4 Plants', *Functional Plant Biology*, 19(5), p. 519. doi: 10.1071/pp9920519.

Comins, H. N. and McMurtrie, R. E. (1993) 'Long-Term Response of Nutrient-Limited Forests to CO"2 Enrichment; Equilibrium Behavior of Plant-Soil Models', *Ecological Applications*, 3(4), pp. 666–681. doi: 10.2307/1942099.

Costa, M. G. *et al.* (2016) 'Labile and Non-Labile Fractions of Phosphorus and Its Transformations in Soil under Eucalyptus', pp. 1–15. doi: 10.3390/f7010015.

Davidson, E. A. *et al.* (2004) 'Nitrogen and phosphorus limitation of biomass growth in a tropical secondary forest', *Ecological Applications*, 14(4 SUPPL.), pp. 150–163. doi: 10.1890/01-6006.

DeLuca, T. H., Keeney, D. R. and McCarty, G. W. (1992) 'Effect of freeze-thaw-events on mineralization of soil nitrogen', *Biol. Fertil. Soils*, 14, pp. 116–120. doi: 10.1007/BF00336260.

Dieter, D., Elsenbeer, H. and Turner, B. L. (2010) 'Phosphorus fractionation in lowland tropical rainforest soils in central Panama.', *Catena*, 82(2), pp. 118–125. doi: 10.1016/j.catena.2010.05.010.

Ellsworth, D. S. *et al.* (2017) 'Elevated $CO_2$ does not increase eucalypt forest productivity on a low-phosphorus soil', *Nature Climate Change*, 7(4), pp. 279–282. doi: 10.1038/nclimate3235.

Elser, J. J. *et al.* (2007) 'Global analysis of nitrogen and phosphorus limitation of primary producers in freshwater, marine and terrestrial ecosystems', *Ecology Letters*, 10(12), pp. 1135–1142. doi: 10.1111/j.1461-0248.2007.01113.x.

Fernández-Martínez, M. *et al.* (2019) 'Global trends in carbon sinks and their relationships with $CO_2$ and temperature', *Nature Climate Change*, 9(1), pp. 73–79. doi: 10.1038/s41558-018-0367-7.

Fleischer, K. *et al.* (2019) 'Amazon forest response to $CO_2$ fertilization dependent on plant phosphorus acquisition', *Nature Geoscience*. doi: 10.1038/s41561-019-0404-9.

Friedlingstein, P. *et al.* (2006) 'Climate-carbon cycle feedback analysis: Results from the C4MIP model intercomparison', *Journal of Climate*, 19(14), pp. 3337–3353. doi: 10.1175/JCLI3800.1.

Friedlingstein, P. *et al.* (2019) 'Comment on "The global tree restoration potential"', *Science*. doi: 10.1126/science.aay8060.

Fyllas, N. M. *et al.* (2009) 'Basin-wide variations in foliar properties of Amazonian forest: phylogeny, soils and climate', *Biogeosciences*, 6(11), pp. 2677–2708. doi: 10.5194/bg-6-2677-2009.

Gentile, R. *et al.* (2012) 'Effects of long-term exposure to enriched $CO_2$ on the nutrient-supplying capacity of a grassland soil', *Biology and Fertility of Soils*, 48(3), pp. 357–362. doi: http://dx.doi.org/10.1007/s00374-011-0616-7.

Goll, D. S. *et al.* (2017) 'A representation of the phosphorus cycle for ORCHIDEE (revision 4520)', *Geoscientific Model Development*, 10(10), pp. 3745–3770. doi: 10.5194/gmd-10-3745-2017.

Gross, A. *et al.* (2021) 'Direct foliar uptake of phosphorus from desert dust', *New Phytologist*, 230(6), pp. 2213–2225. doi: 10.1111/nph.17344.

Harper, A. B. *et al.* (2016) 'Improved representation of plant functional types and physiology in the Joint UK Land Environment Simulator (JULES v4.2) using plant trait information', *Geoscientific Model Development*, 9(7), pp. 2415–2440. doi: 10.5194/gmd-9-2415-2016.

Harris, I. *et al.* (2014) 'Updated high-resolution grids of monthly climatic observations - the CRU TS3.10 Dataset', *International Journal of Climatology*, 34(3), pp. 623–642. doi: 10.1002/joc.3711.

Hatfield, J. L. and Dold, C. (2019) 'Water-use efficiency: Advances and challenges in a changing climate', *Frontiers in Plant Science*, 10(February), pp. 1–14. doi: 10.3389/fpls.2019.00103.

Haverd, V. *et al.* (2018) 'A new version of the CABLE land surface model (Subversion revision r4601) incorporating land use and land cover change, woody vegetation demography, and a novel optimisation-based approach to plant coordination of photosynthesis', *Geoscientific Model Development*, 11(7), pp. 2995–3026. doi: 10.5194/gmd-11-2995-2018.

He, M. and Dijkstra, F. A. (2014) 'Drought effect on plant nitrogen and phosphorus: A meta-analysis', *New Phytologist*, 204(4), pp. 924–931. doi: 10.1111/nph.12952.

Hedley, M. J., Stewart, J. W. B. and Chauhan, B. S. (1982) 'Changes in Inorganic and Organic Soil Phosphorus Fractions Induced by Cultivation Practices and by Laboratory Incubations', *Soil Science Society of America Journal*, 46(5), pp. 970–976. doi: https://doi.org/10.2136/sssaj1982.03615995004600050017x.

Herbert, D. A., Williams, M. and Rastetter, E. B. (2003) 'A model analysis of N and P limitation on carbon accumulation in Amazonian secondary forest after alternate land-use abandonment', *Biogeochemistry*, 65(1), pp. 121–150. doi: 10.1023/A:1026020210887.

Hou, E. *et al.* (2019) 'Quantifying Soil Phosphorus Dynamics: A Data Assimilation Approach', *Journal of Geophysical Research: Biogeosciences*, 124(7), pp. 2159–2173. doi: 10.1029/2018JG004903.

Hou, E. *et al.* (2020) 'Global meta-analysis shows pervasive phosphorus limitation of aboveground plant production in natural terrestrial ecosystems', *Nature Communications*, 11(1), pp. 1–9. doi: 10.1038/s41467-020-14492-w.

Hubau, W. *et al.* (2020) 'Asynchronous carbon sink saturation in African and Amazonian tropical forests', *Nature*, 579(7797), pp. 80–87. doi: 10.1038/s41586-020-2035-0.

Hungate, B. a *et al.* (2003) 'Nitrogen and Climate Change', *Science*, 302(November), pp. 1512–1513.

Jenkinson, D. S. *et al.* (1990) 'The turnover of organic carbon and nitrogen in soil', *The Royal Society*, 329(1255). doi: https://doi.org/10.1098/rstb.1990.0177.

Jenkinson, D. S. and Coleman, K. (2008) 'The turnover of organic carbon in subsoils. Part 2. Modelling carbon turnover', *European Journal of Soil Science*, 59(2), pp. 400–413. doi: 10.1111/j.1365-2389.2008.01026.x.

Ji, D. *et al.* (2014) 'Description and basic evaluation of Beijing Normal University Earth System Model (BNU-

ESM) version 1', *Geoscientific Model Development*, 7(5), pp. 2039–2064. doi: 10.5194/gmd-7-2039-2014.

Jiang, M. *et al.* (2019) 'Towards a more physiological representation of vegetation phosphorus processes in land surface models', *New Phytologist*, 222(3), pp. 1223–1229. doi: 10.1111/nph.15688.

Jiang, M. *et al.* (2020) 'The fate of carbon in a mature forest under carbon dioxide enrichment', *Nature*, 580(7802), pp. 227–231. doi: 10.1038/s41586-020-2128-9.

Jiménez, E. M. *et al.* (2009) 'Fine root dynamics for forests on contrasting soils in the Colombian Amazon', *Biogeosciences*, 6(12), pp. 2809–2827. doi: 10.5194/bg-6-2809-2009.

Johnson, M. O. *et al.* (2016) 'Variation in stem mortality rates determines patterns of above-ground biomass in Amazonian forests: implications for dynamic global vegetation models', *Global Change Biology*, 22(12), pp. 3996–4013. doi: 10.1111/gcb.13315.

Jones, S. *et al.* (2020) 'The impact of a simple representation of non-structural carbohydrates on the simulated response of tropical forests to drought', *Biogeosciences*, 17(13), pp. 3589–3612. doi: 10.5194/bg-17-3589-2020.

Kattge, J. *et al.* (2009) 'Quantifying photosynthetic capacity and its relationship to leaf nitrogen content for global-scale terrestrial biosphere models', *Global Change Biology*, 15(4), pp. 976–991. doi: https://doi.org/10.1111/j.1365-2486.2008.01744.x.

Keller, M. *et al.* (2004) 'Ecological research in the Large-scale Biosphere-Atmosphere Experiment in Amazonia: Early results', *Ecological Applications*, 14(4 SUPPL.), pp. 3–16. doi: 10.1890/03-6003.

Klein, T. *et al.* (2016) 'Growth and carbon relations of mature Picea abies trees under 5 years of free-air CO2 enrichment', *Journal of Ecology*, 104(6), pp. 1720–1733. doi: 10.1111/1365-2745.12621.

Koch, A., Hubau, W. and Lewis, S. L. (2021) 'Earth System Models Are Not Capturing Present-Day Tropical Forest Carbon Dynamics', *Earth's Future*, 9(5), pp. 1–19. doi: 10.1029/2020EF001874.

Körner, C. *et al.* (2005) 'Ecology: Carbon flux and growth in mature deciduous forest trees exposed to elevated CO2', *Science*, 309(5739), pp. 1360–1362. doi: 10.1126/science.1113977.

Van Langenhove, L. *et al.* (2020) 'Atmospheric deposition of elements and its relevance for nutrient budgets of tropical forests', *Biogeochemistry*, 149(2), pp. 175–193. doi: 10.1007/s10533-020-00673-8.

Lapola, D. M. and Norby, R. (2014) 'Assessing the effects of increased atmospheric CO 2 on the ecology and resilience of the Amazon forest', *Science plan et implementation strategy*, AMAZON FAC.

LeBauer, D. and Treseder, K. (2008) 'Nitrogen Limitation of Net Primary Productivity', *Ecology*, 89(2), pp. 371–379.

Lloyd, J. *et al.* (2001) 'Should Phosphorus Availability Be Constraining Moist Tropical Forest Responses to Increasing CO2 Concentrations?', in *Global Biogeochemical Cycles in the Climate System*. Elsevier, pp. 95–114. doi: 10.1016/B978-012631260-7/50010-8.

Long, M. C. *et al.* (2013) 'Twentieth-century oceanic carbon uptake and storage in CESM1(BGC)', *Journal of Climate*, 26(18), pp. 6775–6800. doi: 10.1175/JCLI-D-12-00184.1.

De Lucia, E. H. *et al.* (2007) 'Forest carbon use efficiency: Is respiration a constant fraction of gross primary production?', *Global Change Biology*, 13(6), pp. 1157–1167. doi: 10.1111/j.1365-2486.2007.01365.x.

Lugli, L. F. (2013) *Estoque de nutrientes na serrapilheira fina e grossa em função de fatores edáficos em florestas do Amazonas, Brasil*. Instituto Nacional de Pesquisas da Amazônia - INPA. Available at: https://repositorio.inpa.gov.br/handle/1/5028.

Lugli, L. F. *et al.* (2020) 'Multiple phosphorus acquisition strategies adopted by fine roots in low-fertility soils in Central Amazonia', *Plant and Soil*, 450(1–2), pp. 49–63. doi: 10.1007/s11104-019-03963-9.

Lugli, L. F. *et al.* (2021) 'Rapid responses of root traits and productivity to phosphorus and cation additions in a tropical lowland forest in Amazonia', *New Phytologist*, 230(1), pp. 116–128. doi: 10.1111/nph.17154.

Luo, Y. *et al.* (2004) 'Progressive nitrogen limitation of ecosystem responses to rising atmospheric carbon dioxide', *BioScience*, 54(8), pp. 731–739. doi: 10.1641/0006-3568(2004)054[0731:PNLOER]2.0.CO;2.

Malhi, Y. *et al.* (2004) 'The above-ground coarse wood productivity of 104 Neotropical forest plots', *Global Change Biology*, 10(5), pp. 563–591. doi: 10.1111/j.1529-8817.2003.00778.x.

Malhi, Y. *et al.* (2006) 'The regional variation of aboveground live biomass in old-growth Amazonian forests', *Global Change Biology*, 12(7), pp. 1107–1138. doi: 10.1111/j.1365-2486.2006.01120.x.

Malhi, Y. *et al.* (2009) 'Comprehensive assessment of carbon productivity, allocation and storage in three Amazonian forests', *Global Change Biology*, 15(5), pp. 1255–1274. doi: 10.1111/j.1365-2486.2008.01780.x.

Malhi, Y. (2012) 'The productivity, metabolism and carbon cycle of tropical forest vegetation', *Journal of Ecology*, 100(1), pp. 65–75. doi: 10.1111/j.1365-2745.2011.01916.x.

Malhi, Y., Doughty, C. and Galbraith, D. (2011) 'The allocation of ecosystem net primary productivity in tropical forests', *Philosophical Transactions of the Royal Society B: Biological Sciences*, 366(1582), pp. 3225–3245. doi: 10.1098/rstb.2011.0062.

Martins, N. P. *et al.* (2021) 'Fine roots stimulate nutrient release during early stages of leaf litter decomposition in a Central Amazon rainforest', *Plant and Soil*, 469(1–2), pp. 287–303. doi: 10.1007/s11104-021-05148-9.

Medlyn, B. E. *et al.* (2015) 'Using ecosystem experiments to improve vegetation models', *Nature Climate Change*, 5(6), pp. 528–534. doi: 10.1038/nclimate2621.

1294 Medlyn, B. E. *et al.* (2016) 'Using models to guide field experiments: a priori predictions for the CO2 response
1295 of a nutrient- and water-limited native Eucalypt woodland', *Global Change Biology*, 22(8), pp. 2834–2851. doi:
1296 10.1111/gcb.13268.
1297 Mercado, L. M. *et al.* (2011) 'Variations in Amazon forest productivity correlated with foliar nutrients and
1298 modelled rates of photosynthetic carbon supply', *Philosophical Transactions of the Royal Society B: Biological*
1299 *Sciences*, 366(1582), pp. 3316–3329. doi: 10.1098/rstb.2011.0045.
1300 Mirabello, M. J. *et al.* (2013) 'Soil phosphorus responses to chronic nutrient fertilisation and seasonal drought in
1301 a humid lowland forest, Panama', *Soil Research*, 51(3), pp. 215–221. doi: 10.1071/SR12188.
1302 Mitchard, E. T. A. (2018) 'The tropical forest carbon cycle and climate change', *Nature*, 559(7715), pp. 527–
1303 534. doi: 10.1038/s41586-018-0300-2.
1304 Nachtergaele, F. *et al.* (2010) 'The Harmonized World Soil Database', *Proceedings of the 19th World Congress*
1305 *of Soil Science, Soil Solutions for a Changing World, Brisbane, Australia, 1-6 August 2010*, pp. 34–37. doi:
1306 3123.
1307 Neff, J. C., Hobbie, S. E. and Vitousek, P. M. (2000) 'Nutrient and mineralogical control on dissolved organic
1308 C, N and P fluxes and stoichiometry in Hawaiian soils', *Biogeochemistry*, 51(3), pp. 283–302. doi:
1309 10.1023/A:1006414517212.
1310 Norby, R. J. *et al.* (2016) 'Model–data synthesis for the next generation of forest free-air <scp>CO</scp> 2
1311 enrichment ( <scp>FACE</scp> ) experiments', *New Phytologist*, 209(1), pp. 17–28. doi: 10.1111/nph.13593.
1312 Nordin, A., Högberg, P. and Näsholm, T. (2001) 'Soil nitrogen form and plant nitrogen uptake along a boreal
1313 forest productivity gradient', *Oecologia*, 129(1), pp. 125–132. doi: 10.1007/s004420100698.
1314 Pan, Y. *et al.* (2011) 'A Large and Persistent Carbon Sink in the World's Forests', *Science*, 333(6045), pp. 988–
1315 993. doi: 10.1126/science.1201609.
1316 Perakis, S. S. and Hedin, L. O. (2002) 'Nitrogen loss from unpolluted South American forests mainly via
1317 dissolved organic compounds', *Nature*, 415(6870), pp. 416–419. doi: 10.1038/415416a.
1318 Phillips, O. L. *et al.* (2004) 'Pattern and process in Amazon tree turnover, 1976-2001', *Philosophical*
1319 *Transactions of the Royal Society B: Biological Sciences*, 359(1443), pp. 381–407. doi: 10.1098/rstb.2003.1438.
1320 Phillips, O. L. *et al.* (2017) 'Carbon uptake by mature Amazon forests has mitigated Amazon nations' carbon
1321 emissions', *Carbon Balance and Management*, 12(1), pp. 1–9. doi: 10.1186/s13021-016-0069-2.
1322 Pyle, E. H. *et al.* (2009) 'Dynamics of carbon, biomass, and structure in two Amazonian forests', *Journal of*
1323 *Geophysical Research: Biogeosciences*, 114(1), pp. 1–20. doi: 10.1029/2007JG000592.
1324 Quesada, C. A. *et al.* (2010) 'Variations in chemical and physical properties of Amazon forest soils in relation to
1325 their genesis', *Biogeosciences*, 7(5), pp. 1515–1541. doi: 10.5194/bg-7-1515-2010.
1326 Quesada, C. A. *et al.* (2011) 'Soils of Amazonia with particular reference to the RAINFOR sites',
1327 *Biogeosciences*, 8(6), pp. 1415–1440. doi: 10.5194/bg-8-1415-2011.
1328 Quesada, C. A. *et al.* (2012) 'Basin-wide variations in Amazon forest structure and function are mediated by
1329 both soils and climate', *Biogeosciences*, 9(6), pp. 2203–2246. doi: 10.5194/bg-9-2203-2012.
1330 Reed, S. C., Yang, X. and Thornton, P. E. (2015) 'Incorporating phosphorus cycling into global modeling
1331 efforts: A worthwhile, tractable endeavor', *New Phytologist*, 208(2), pp. 324–329. doi: 10.1111/nph.13521.
1332 Ryan, M. G. (2013) 'Three decades of research at Flakaliden advancing whole-tree physiology, forest ecosystem
1333 and global change research', *Tree Physiology*, 33(11), pp. 1123–1131. doi: 10.1093/treephys/tpt100.
1334 Sampaio, G. *et al.* (2021) 'CO2physiological effect can cause rainfall decrease as strong as large-scale
1335 deforestation in the Amazon', *Biogeosciences*, 18(8), pp. 2511–2525. doi: 10.5194/bg-18-2511-2021.
1336 Sanchez, P. A. (1977) 'Properties and Management of Soils in the Tropics', *Soil Science*, 124(3). Available at:
1337 https://journals.lww.com/soilsci/Fulltext/1977/09000/Properties_and_Management_of_Soils_in_the_Tropics.12.
1338 aspx.
1339 Sardans, J., Rivas-Ubach, A. and Peñuelas, J. (2012) 'The C:N:P stoichiometry of organisms and ecosystems in
1340 a changing world: A review and perspectives', *Perspectives in Plant Ecology, Evolution and Systematics*, 14(1),
1341 pp. 33–47. doi: 10.1016/j.ppees.2011.08.002.
1342 Schimel, D., Stephens, B. B. and Fisher, J. B. (2015) 'Effect of increasing CO2 on the terrestrial carbon cycle',
1343 *Proceedings of the National Academy of Sciences of the United States of America*, 112(2), pp. 436–441. doi:
1344 10.1073/pnas.1407302112.
1345 Shen, J. *et al.* (2011) 'Phosphorus dynamics: From soil to plant', *Plant Physiology*, 156(3), pp. 997–1005. doi:
1346 10.1104/pp.111.175232.
1347 Sitch, S. *et al.* (2008) 'Evaluation of the terrestrial carbon cycle, future plant geography and climate-carbon
1348 cycle feedbacks using five Dynamic Global Vegetation Models (DGVMs)', *Global Change Biology*, 14(9), pp.
1349 2015–2039. doi: 10.1111/j.1365-2486.2008.01626.x.
1350 Stephenson, N. L. and Van Mantgem, P. J. (2005) 'Forest turnover rates follow global and regional patterns of
1351 productivity', *Ecology Letters*, 8(5), pp. 524–531. doi: 10.1111/j.1461-0248.2005.00746.x.
1352 Sun, Y. *et al.* (2021) 'Global evaluation of the nutrient-enabled version of the land surface model ORCHIDEE-
1353 CNP v1.2 (r5986)', *Geoscientific Model Development*, 14(4), pp. 1987–2010. doi: 10.5194/gmd-14-1987-2021.

1354 Turner, B. L. *et al.* (2015) 'Seasonal changes in soil organic matter after a decade of nutrient addition in a
1355 lowland tropical forest', *Biogeochemistry*, 123(1–2), pp. 221–235. doi: 10.1007/s10533-014-0064-1.
1356 Turner, B. L. and Condron, L. M. (2013) 'Pedogenesis, nutrient dynamics, and ecosystem development: the
1357 legacy of T.W. Walker and J.K. Syers', *Plant and Soil*, 367(1–2), pp. 1–10. doi: 10.1007/s11104-013-1750-9.
1358 Vicca, S. *et al.* (2012a) 'Fertile forests produce biomass more efficiently', *Ecology Letters*, 15(6), pp. 520–526.
1359 doi: 10.1111/j.1461-0248.2012.01775.x.
1360 Vicca, S. *et al.* (2012b) 'Fertile forests produce biomass more efficiently', *Ecology Letters*, 15(6), pp. 520–526.
1361 doi: 10.1111/j.1461-0248.2012.01775.x.
1362 Vitousek, P. M. *et al.* (1997) 'Human Domination of Earth Ecosystems', *Science*, 278(5335), p. 21. Available
1363 at: http://www.cheric.org/research/tech/periodicals/view.php?seq=257860.
1364 Vitousek, P. M. (2004) *Nutrient Cycling and Limitation: Hawai'i as a Model System*. Princeton University Press
1365 (Princeton Environmental Institute series). Available at:
1366 https://books.google.com.fj/books?id=6EmAtAEACAAJ.
1367 Vitousek, P. M. *et al.* (2010) 'Terrestrial phosphorus limitation: Mechanisms, implications, and nitrogen-
1368 phosphorus interactions', *Ecological Applications*, 20(1), pp. 5–15. doi: 10.1890/08-0127.1.
1369 Vitousek, P. M. and Howarth, R. W. (1991) 'Nitrogen limitation on land and in the sea: How can it occur?',
1370 *Biogeochemistry*, 13(2), pp. 87–115. doi: 10.1007/BF00002772.
1371 Walker, A. P. *et al.* (2021) 'Integrating the evidence for a terrestrial carbon sink caused by increasing
1372 atmospheric CO2', *New Phytologist*, 229(5), pp. 2413–2445. doi: 10.1111/nph.16866.
1373 Walker, T. W. and Syers, J. K. (1976) 'The fate of phosphorus during pedogenesis', *Geoderma*, 15(1), pp. 1–19.
1374 doi: 10.1016/0016-7061(76)90066-5.
1375 Wang, Y. P., Houlton, B. Z. and Field, C. B. (2007) 'A model of biogeochemical cycles of carbon, nitrogen, and
1376 phosphorus including symbiotic nitrogen fixation and phosphatase production', *Global Biogeochemical Cycles*,
1377 21(1), pp. 1–15. doi: 10.1029/2006GB002797.
1378 Wang, Y. P., Law, R. M. and Pak, B. (2010) 'A global model of carbon, nitrogen and phosphorus cycles for the
1379 terrestrial biosphere', *Biogeosciences*, 7(7), pp. 2261–2282. doi: 10.5194/bg-7-2261-2010.
1380 Went, F. W. and Stark, N. (1968) 'Mycorrhiza', *BioScience*, 18(11), pp. 1035–1039. doi: 10.2307/1294552.
1381 Wiltshire, A. J. *et al.* (2020) 'JULES-CN : a coupled terrestrial Carbon-Nitrogen Scheme ( JULES vn5 . 1 )',
1382 (July), pp. 1–40.
1383 Wiltshire, A. J. *et al.* (2021) 'Jules-cn: A coupled terrestrial carbon-nitrogen scheme (jules vn5.1)',
1384 *Geoscientific Model Development*, 14(4), pp. 2161–2186. doi: 10.5194/gmd-14-2161-2021.
1385 Wright, S. J. *et al.* (2011) 'Potassium, phosphorus, or nitrogen limit root allocation, tree growth, or litter
1386 production in a lowland tropical forest', *Ecology*, 92(8), pp. 1616–1625. doi: 10.1890/10-1558.1.
1387 Xiao, J. *et al.* (2013) 'Carbon fluxes, evapotranspiration, and water use efficiency of terrestrial ecosystems in
1388 China', *Agricultural and Forest Meteorology*, 182–183, pp. 76–90. doi: 10.1016/j.agrformet.2013.08.007.
1389 Xu, Z. *et al.* (2016) 'Elevated-CO2 response of stomata and its dependence on environmental factors', *Frontiers*
1390 *in Plant Science*, 7(MAY2016), pp. 1–15. doi: 10.3389/fpls.2016.00657.
1391 Yang, X. *et al.* (2013) 'The distribution of soil phosphorus for global biogeochemical modeling',
1392 *Biogeosciences*, 10(4), pp. 2525–2537. doi: 10.5194/bg-10-2525-2013.
1393 Yang, X. *et al.* (2014) 'The role of phosphorus dynamics in tropical forests – a modeling study using CLM-
1394 CNP', *Biogeosciences*, 11(6), pp. 1667–1681. doi: 10.5194/bg-11-1667-2014.
1395 Yang, X. and Post, W. M. (2011) 'Phosphorus transformations as a function of pedogenesis: A synthesis of soil
1396 phosphorus data using Hedley fractionation method', *Biogeosciences*, 8(10), pp. 2907–2916. doi: 10.5194/bg-8-
1397 2907-2011.
1398 Zaehle, S. and Dalmonech, D. (2011) 'Carbon-nitrogen interactions on land at global scales: Current
1399 understanding in modelling climate biosphere feedbacks', *Current Opinion in Environmental Sustainability*,
1400 3(5), pp. 311–320. doi: 10.1016/j.cosust.2011.08.008.
1401 Zaehle, S. and Friend, A. D. (2010) 'Carbon and nitrogen cycle dynamics in the O-CN land surface model: 1.
1402 Model description, site-scale evaluation, and sensitivity to parameter estimates', *Global Biogeochemical Cycles*,
1403 24(1), pp. 1–13. doi: 10.1029/2009GB003521.
1404 Zhu, Q. *et al.* (2016) 'Multiple soil nutrient competition between plants, microbes, and mineral surfaces: model
1405 development, parameterization, and example applications in several tropical forests', *Biogeosciences*, 13(1), pp.
1406 341–363. doi: 10.5194/bg-13-341-2016.
1407